

Strong Two-Body Decays of Light Mesons

Ralf Ricken, Matthias Koll*, Dirk Merten, Bernard C. Metsch

— June 2, 2018 —

In this paper, we present results on strong two-body decay widths of light $q\bar{q}$ mesons calculated in a covariant quark model. The model is based on the Bethe-Salpeter equation in its instantaneous approximation and has already been used for computing the complete meson mass spectrum and many electroweak decay observables. Our approach relies on the use of a phenomenological confinement potential with an appropriate spinorial Dirac structure and 't Hooft's instanton-induced interaction as a residual force for pseudoscalar and scalar mesons.

The transition matrix element for the decay of one initial meson into two final mesons is evaluated in lowest order by considering conventional decays via quark loops as well as Zweig rule violating instanton-induced decays generated by the six-quark vertex of 't Hooft's interaction; the latter mechanism only contributes if all mesons in the decay have zero total angular momentum. We show that the interference of both decay mechanisms plays an important role in the description of the partial widths of scalar and pseudoscalar mesons.

1 Introduction

The study of the internal structure of mesons is still a challenge to theoretical physics as well as to experimental physics. Despite all efforts undertaken in the last decades, in particular the strong decays of $q\bar{q}$ bound states are rather poorly understood. For theory, one of the reasons might be related to the fact that — at least for the sector of mesons being composed out of light quarks — a relativistic treatment of the underlying dynamics seems to be mandatory. In principle, this requirement is satisfied by a study of strong two-body decays on the basis of the Bethe-Salpeter equation in its instantaneous approximation. However, the particular structure of the full transition operator for this class of mesonic decays is quite unclear even in a covariant framework. In the present work, we suppose that the pure quark loop contribution present in all strong decays is accompanied by an additional instanton-induced decay mechanism if and only if all mesons in the process have a vanishing total angular momentum.

Before we discuss our approach to the problem of strong two-body decays of light mesons in detail, let us briefly make some remarks on a non-relativistic phenomenological model which is quite prominent in this field, namely the so-called 3P_0 model. It has its origins in the early works of A. Le Yaouanc *et al.* published in refs. [1, 2, 3] (see also [4]). As has been suggested earlier by L. Micu (see [5]), the authors assume that these two-body strong decays proceed via the creation of a $q\bar{q}$ state with vacuum quantum numbers $J^{\pi c} = 0^{++}$; the equivalent spectroscopic notation for $q\bar{q}$ bound states reads ${}^{2S+1}L_J = {}^3P_0$ which has in fact labeled this particular model. In ref. [6], T. Barnes *et al.* have reviewed the results of the modern 3P_0 model with respect to strong two-body decays and compared the results to the (rare and ambiguous) experimental data for light $n\bar{n}$ ground-state mesons; higher quarkonia are studied in ref. [7]. For completeness, we should also mention the recently published work of R. Bonnaz and B. Silvestre-Brac who include instanton induced effects as well as tensor forces in their study on the basis of the 3P_0 model (see [8] and references therein); for decays of non- $n\bar{n}$ meson states, we will refer to their results.¹

Our Bethe-Salpeter approach has first been discussed in refs. [9, 10]; recently, we have presented an updated review concerning meson spectra and electroweak decay characteristics (see [11, 12]). In the present paper, we aim at a rather complete description of strong two-body decays of light mesons in the framework of our relativistic quark model. Our approach is furthermore interesting insofar as we not only compute the quark loop contribution but also an instanton-induced term for $J_i = 0$ mesons as well as the interference of both

*e-mail address: koll@itkp.uni-bonn.de

¹Note that a recent preprint by Barnes *et al.* (see [39]) also investigates the non- $n\bar{n}$ meson decays; we comment on this work in section 4.

mechanism; note that the latter interaction has already been studied separately in ref. [13] by Ch. Ritter *et al.* for the present relativistic framework.

For the following comprehensive discussion, we compare our results with the available experimental data compiled by the PARTICLE DATA GROUP (see [14]; additional results can be found in [15, 16, 17, 18, 19]) on the one hand as well as with the results of the 3P_0 model presented in refs. [6, 7, 8] on the other hand. Thus, we understand the current work as a reference frame for a more reliable assessment of the multifaceted (and partly contradicting) results on strong two-body decays of light mesons.

We have organized this contribution as follows: in section 2, we briefly review our covariant approach on the basis of the Bethe–Salpeter equation in its instantaneous approximation; furthermore, we comment on the results concerning the light meson spectra (see also [11, 12]). The transition matrix element for strong decays of the type $\mathcal{M}_1 \rightarrow \mathcal{M}_2 \mathcal{M}_3$ is derived in section 3; as mentioned above, it includes an instanton–induced contribution for scalar and pseudoscalar mesons beyond the lowest order quark loop part. Our results for numerous decays are presented and discussed in section 4. Finally, we give a summary of our work in section 5. The appendix includes technical details concerning the flavour matrix elements and G. ’t Hooft’s instanton–induced interaction following refs. [20, 21, 22].

2 A Relativistic Quark Model for Mesons

In our approach, we treat the (constituent) quarks as fundamental degrees of freedom for the description of hadronic bound states. The resulting quark model is formally covariant and relies basically on the instantaneous Bethe–Salpeter equation. It has been reviewed in detail in refs. [11, 12] such that we can keep the following introduction rather compact before we turn to the strong decay matrix elements in the next section.

2.1 The instantaneous Bethe–Salpeter approach

In quantum field theory, a quark–anti-quark bound state with four-momentum P and mass M ($M^2 = P^2$) is described by the Bethe–Salpeter equation for two fermions (see [23]). In momentum space, this equation reads

$$\chi^P(p) = -i S_1^F \left(\frac{P}{2} + p \right) \left[\int \frac{d^4 p'}{(2\pi)^4} K(P, p, p') \chi^P(p') \right] S_2^F \left(-\frac{P}{2} + p \right) \quad (1)$$

where p is the relative four-momentum between the quark and the anti-quark, K denotes the infinite sum of their irreducible interactions and the corresponding full Feynman propagators are labeled by S_1^F and S_2^F , respectively. The Bethe–Salpeter amplitude χ^P is defined in coordinate space as the time-ordered product of the quark and the anti-quark field operator between the bound state $|P\rangle$ and the vacuum:

$$\begin{aligned} \chi_{\alpha\beta}^P(x_1, x_2) &:= \langle 0 | \mathcal{T} \psi_\alpha^1(x_1) \bar{\psi}_\beta^2(x_2) | P \rangle \\ &= e^{-iP \cdot (x_1 + x_2)/2} \int \frac{d^4 p}{(2\pi)^4} e^{-ip \cdot (x_1 - x_2)} \chi_{\alpha\beta}^P(p) \end{aligned} \quad (2)$$

where α and β are multi-indices for the Dirac, flavour and colour degrees of freedom which are omitted in the following discussion. Since in general the interaction kernel K and the full quark propagators S_i^F are unknown quantities, we make two (formally covariant) approximations:

- The propagators are assumed to be of the free form $S_i^F = i(\not{p} - m_i + i\epsilon)^{-1}$ with effective constituent quark masses m_i that we consider as free parameters in our model; thus, all dynamical self-interactions of the (anti-)quarks are believed to be adequately parameterized by a constant absorbed in the constituent masses.
- The interaction kernel shall only depend on the components of p and p' perpendicular to P , *i.e.* we assume that $K(P, p, p') = V(p_{\perp P}, p'_{\perp P})$ with $p_{\parallel P} := (p \cdot P/P^2)P$ and $p_{\perp P} := p - p_{\parallel P}$ holds; therefore, the interaction kernel in the meson rest frame with $P_M = (M, \vec{0})$ becomes independent of the variable $p_{\parallel P_M} \equiv p^0$ which is the reason for labelling this assumption the “instantaneous approximation”.

Integrating in the bound state rest frame over the relative energy p^0 and introducing the equal-time amplitude (or Salpeter amplitude) $\Phi(\vec{p}) := \int \frac{dp^0}{2\pi} \chi^P(p^0, \vec{p})|_{P=(M, \vec{0})}$, we end up with the Salpeter equation (see [24]) which constitutes the basic equation of our model:

$$\Phi(\vec{p}) = +\Lambda_1^-(\vec{p}) \gamma^0 \left[\int \frac{d^3 p'}{(2\pi)^3} \frac{V(\vec{p}, \vec{p}') \Phi(\vec{p}')}{{M + \omega_1 + \omega_2}} \right] \gamma^0 \Lambda_2^+(-\vec{p})$$

$$-\Lambda_1^+(\vec{p})\gamma^0 \left[\int \frac{d^3p'}{(2\pi)^3} \frac{V(\vec{p}, \vec{p}')\Phi(\vec{p}')}{M - \omega_1 - \omega_2} \right] \gamma^0 \Lambda_2^-(\vec{p}) . \quad (3)$$

Here, $\Lambda_i^\pm(\vec{p}) = \frac{1}{2} \pm \gamma^0(\vec{\gamma} \cdot \vec{p} + m_i)/2\omega_i$ are projectors on positive and negative energy solutions of the Dirac equation and $\omega_i = \sqrt{\vec{p}^2 + m_i^2}$ denotes the kinetic energy of the quarks. The simultaneous calculation of the meson masses M and the Salpeter amplitudes Φ results by solving the corresponding eigenvalue problem of eq. (3) with an adequate potential ansatz (see [9, 11] for further details).

The calculation of transition matrix elements for decays or scattering processes can be done in the Mandelstam formalism (see [25]). To this end, the full Bethe–Salpeter amplitude $\chi^P(p)$ depending on the relative four-momentum p has to be known. On the mass shell of the bound state, it can be reconstructed from the Salpeter amplitude $\Phi(\vec{p})$ in a covariant manner. Let us therefore first define the meson–quark–antiquark vertex function $\Gamma^P(p) := [S_1^F(P/2 + p)]^{-1} \chi^P(p) [S_2^F(-P/2 + p)]^{-1}$ as the amputated Bethe–Salpeter amplitude. Starting with the corresponding amputated Bethe–Salpeter equation, the vertex function in the meson’s rest frame can be computed from the three-dimensional Salpeter amplitude by

$$\Gamma(\vec{p}) := \Gamma^P(p)|_{P=(M, \vec{0})} = -i \int \frac{d^3p'}{(2\pi)^3} V(\vec{p}, \vec{p}') \Phi(\vec{p}') . \quad (4)$$

Due to covariance of this procedure, we can finally calculate the Bethe–Salpeter amplitude for any on–shell momentum $P' = (P'_0, \vec{P}')$ of the bound state by performing a pure boost Λ according to

$$\chi^{P'}(p) = S_\Lambda \chi^P(\Lambda^{-1}p) S_\Lambda^{-1} \quad \text{with} \quad \chi^P(p) = \chi^P(p_0, \vec{p}) = S_1^F\left(\frac{M}{2} + p_0, \vec{p}\right) \Gamma(\vec{p}) S_2^F\left(-\frac{M}{2} + p_0, \vec{p}\right) \quad (5)$$

where S_Λ denotes the corresponding transformation in Dirac space and the boost is defined by $\Lambda P = P'$ for a total momentum $P = (M, \vec{0})$ in the rest frame of the bound state.

2.2 Interactions, Parameters and Spectra

Up to now, we have not specified the interactions that we will include in the instantaneous interaction kernel. From phenomenological studies of QCD, one finds that a confining interaction is mandatory for a satisfying description of low–energy hadrons and especially of their radially excited states. Furthermore, it is clear that an additional interaction should be included in the discussion as a flavour–dependent force is required at least in the sector with total angular momentum $J = 0$. Our candidate for this residual interaction will be ’t Hooft’s instanton–induced force (see appendix B.1). Let us briefly comment on both types of interactions:

- The confining interaction in coordinate space is mostly parameterized as a linearly rising potential of the form $\mathcal{V}_C(r) = a_c + b_c \cdot r$. Moreover, one also has to choose a particular spinorial structure $\Gamma \otimes \Gamma$ for the confining interaction that acts in Dirac space and is *a priori* unknown.

Accordingly, the confining interaction in momentum space acting on the Salpeter amplitude can be written as

$$\int \frac{d^3p'}{(2\pi)^3} V_C(\vec{p}, \vec{p}') \Phi(\vec{p}') = \int \frac{d^3p'}{(2\pi)^3} \tilde{\mathcal{V}}_C((\vec{p} - \vec{p}')^2) \cdot \Gamma \Phi(\vec{p}') \Gamma \quad (6)$$

where $\tilde{\mathcal{V}}_C((\vec{p} - \vec{p}')^2)$ is the Fourier transform of the linear potential $\mathcal{V}_C(r)$ in coordinate space. Note that the offset a_c and the slope b_c will be treated as free parameters in our model.

- As it has been shown in the framework of a non–relativistic quark model (see [26, 27]), the instanton–induced interaction on the basis of the ideas of ’t Hooft and others (see [20, 21, 22]) provides a remarkably good explanation for the ground state masses in the pseudoscalar sector; in a relativistic formulation, ’t Hooft’s force also acts in the scalar meson sector.

In momentum space, the effective potential for the instanton–induced interaction (abbr.: III) can be written as

$$\int \frac{d^3p'}{(2\pi)^3} V_{\text{III}}(\vec{p}, \vec{p}') \Phi(\vec{p}') = 4G(g, g') \int \frac{d^3p'}{(2\pi)^3} \mathcal{R}_\Lambda(\vec{p}, \vec{p}') \cdot (\mathbb{1} \text{tr}[\Phi(\vec{p}')] + \gamma_5 \text{tr}[\gamma_5 \Phi(\vec{p}')]) \quad (7)$$

where $\Lambda = \Lambda_{\text{III}}$ denotes the finite effective range of the force and the regulator function is of Gaussian type, *i.e.* it reads $\mathcal{R}_\Lambda(\vec{x}) = \exp(-|\vec{x}|^2/\Lambda^2)/(\Lambda\sqrt{\pi})^3$ in configuration space. The matrix $G(g, g')$ includes flavour dependent coupling constants g and g' ; a summation over flavour indices is implicitly understood (see appendix B.1 for more details). We will consider the effective range and the coupling constants of 't Hooft's force as free parameters.

We have shown in refs. [11, 12] that these assumptions on the underlying interactions between the constituents of the mesons produce a consistent picture of the complete light meson sector.² The parameters that we have introduced in these former publications were summarized in two sets denoted by “ \mathcal{A} ” and “ \mathcal{B} ”, respectively. In this work, we will only refer to a unique parameter set for the sake of clarity, namely model \mathcal{B} ; the specific numerical values for the corresponding parameters are displayed in tab. 1. At this point, let us stress that we do not alter these parameters which are uniquely fixed to the meson mass spectrum (see [11, 12]). Thus, the following results on strong decay widths can be considered as (quasi) parameter-free predictions insofar as only the three-body 't Hooft coupling $g_{\text{eff}}^{(3)}$ has to be fixed to a selected decay with $J_i = 0$ ($i = 1, 2, 3$); this particular coupling constant appears here for the first time in our model (see also section 4.1). However, we do not aim at a high-precision prediction of strong decay widths with our approach; instead, we consider this work merely as a global overview including qualitative as well as quantitative features and thus providing a reliable framework for future efforts in this field.

In refs. [11, 12], we have thoroughly discussed our results on the mass spectra in the light meson sector. Concerning the ground states, we obtained an excellent description of the well-known Regge trajectories up to highest angular momenta. The combination of the particular spinorial structure of the confinement force in our model and the effects of 't Hooft's instanton-induced interaction provides very good results for the pseudoscalar mass spectrum; concerning the scalar sector, we observe a plausible classification of $q\bar{q}$ mesons even for the first excited states (see [12] for details). In general, the ground states as well as the radial excitations in the isovector, isodoublet and isoscalar sectors are reasonably well described with the parameters given in tab. 1 such that we consider our calculation of the complete light meson mass spectrum as a good starting point for the study of the strong decays of these bound states.

3 The Transition Matrix Element

For the description of the decay of an initial meson with four-momentum P_1 into two final mesons with four-momenta P_2 and P_3 , respectively, we consider the transition matrix element

$$T_{P_1 \rightarrow P_2 P_3} = \langle P_2 P_3 | T | P_1 \rangle . \quad (8)$$

As we will show in the following, the so-called Mandelstam formalism (see [25]) allows for the calculation of any dynamical bound state observable from the corresponding Bethe-Salpeter amplitudes.

3.1 The Six-Point Green's Function

The decay of one initial meson into two final mesons proceeds via an interaction of six (anti-)quarks. Let us therefore define the corresponding six-point Green's function in coordinate space according to

$$G_{\alpha\alpha',\beta\beta',\gamma\gamma'}^{(6)}(x_1, x_2, y_1, y_2, z_1, z_2) := \langle 0 | T \Psi_{\alpha'}(y_1) \bar{\Psi}_{\beta'}(y_2) \Psi_{\gamma'}(z_2) \bar{\Psi}_{\gamma}(z_1) \Psi_{\beta}(x_2) \bar{\Psi}_{\alpha}(x_1) | 0 \rangle . \quad (9)$$

For the following discussion, it is helpful to introduce furthermore the four-point Green's function

$$G_{\alpha_1\alpha_1',\beta_1\beta_1'}^{(4)}(x'_1, x'_2, x_1, x_2) := -\langle 0 | T \Psi_{\alpha_1}(x'_1) \bar{\Psi}_{\beta_1}(x'_2) \Psi_{\beta}(x_2) \bar{\Psi}_{\alpha}(x_1) | 0 \rangle \quad (10)$$

as well as the eight-point Green's function given by

$$\begin{aligned} & G_{\alpha'\alpha'_1,\beta'\beta'_1,\gamma\gamma_1,\gamma'\gamma'_1}^{(8)}(y_1, y_2, z_1, z_2, y'_1, y'_2, z'_1, z'_2) \\ & := -\langle 0 | T \Psi_{\alpha'}(y_1) \bar{\Psi}_{\gamma}(z_1) \Psi_{\gamma_1}(z'_1) \bar{\Psi}_{\alpha'_1}(y'_1) \Psi_{\gamma'}(z_2) \bar{\Psi}_{\beta'}(y_2) \Psi_{\beta'_1}(y'_2) \bar{\Psi}_{\gamma'_1}(z'_2) | 0 \rangle . \end{aligned} \quad (11)$$

²Note that a similar model for baryons described a qqq states has been presented in refs. [28, 29, 30] by U. Löring *et al.*; the authors also use the instantaneous Bethe-Salpeter equation and adopt a confining force plus a residual instanton-induced interaction.

Here, the full Heisenberg field operators Ψ and $\bar{\Psi}$ are labeled with multi-indices α, β, \dots referring to Dirac, flavour and colour space. In these definitions of the n -point Green's functions $G^{(n)}$, the symbol T denotes the time-ordering operator.

In order to connect the full six-point Green's function with the bound state Bethe-Salpeter amplitudes of the three mesons, we first decompose $G^{(6)}$ into a kernel $K^{(6)}$ which is irreducible with respect to the four-point Green's function $G^{(4)}$ of the incoming $\bar{q}q$ pair and the eight-point Green's function $G^{(8)}$ of the two outgoing $\bar{q}q$ pairs:

$$G_{\alpha\alpha',\beta\beta',\gamma\gamma'}^{(6)}(x_1, x_2, y_1, y_2, z_1, z_2) = \int d^4x'_1 d^4x'_2 d^4y'_1 d^4y'_2 d^4z'_1 d^4z'_2 G_{\alpha'\alpha'_1, \beta'\beta'_1, \gamma\gamma_1, \gamma'\gamma'_1}^{(8)}(y_1, y_2, z_1, z_2, y'_1, y'_2, z'_1, z'_2) \times K_{\alpha_1\alpha'_1, \beta_1\beta'_1, \gamma_1\gamma'_1}^{(6)}(x'_1, x'_2, y'_1, y'_2, z'_1, z'_2) G_{\alpha_1\alpha', \beta_1\beta'}^{(4)}(x'_1, x'_2, x_1, x_2). \quad (12)$$

This equation defines the six-point kernel $K^{(6)}$; in fig. 1, we give a diagrammatical representation of this decomposition.

The four-point Green's function $G^{(4)}$ describes the propagation of a $q\bar{q}$ pair within the space-time region where it is created from and annihilated into the vacuum. As we want to calculate the decay of a meson, we are interested in those contributions to $G^{(4)}$ that originate from $q\bar{q}$ bound states denoted by $|P_i\rangle$. Here and in the following, P_i and M_i denote the four-momentum and the mass of the bound state “ i ” with $P_i^2 = M_i^2$; the Fock states $|P_i\rangle$ are normalized according to

$$\langle P_i | P'_i \rangle = (2\pi)^3 2\omega_{P_i} \delta(\vec{P}_i - \vec{P}'_i) \quad \text{with} \quad \omega_{P_i} := P_i^0 = \sqrt{M^2 + \vec{P}_i^2}. \quad (13)$$

Assuming the time-ordering $x_1^0, x_2^0 < x'_1^0, x'_2^0$, a complete set of these states can be inserted into $G^{(4)}$ such that the bound state contribution to the four-point Green's function is given by

$$\begin{aligned} \tilde{G}_{\alpha_1\alpha', \beta_1\beta'}^{(4)}(x'_1, x'_2, x_1, x_2) &:= - \int d\tilde{P}_1 \langle 0 | T\Psi_{\alpha_1}(x'_1) \bar{\Psi}_{\beta_1}(x'_2) | P_1 \rangle \langle P_1 | \mathsf{T} \Psi_{\beta}(x_2) \bar{\Psi}_{\alpha}(x_1) | 0 \rangle \\ &= - \int d\tilde{P}_1 \chi_{\alpha_1\beta_1}^{P_1}(x'_1, x'_2) \bar{\chi}_{\beta\alpha}^{P_1}(x_1, x_2) \end{aligned} \quad (14)$$

with the definition $d\tilde{P} := d^3P / ((2\pi)^3 2\omega_P)$. Note that we have used the definition of the Bethe-Salpeter amplitude χ according to eq. (2); an analogous definition holds for the adjoint amplitude $\bar{\chi}$.

In order to express also the eight-point Green's function $G^{(8)}$ by Bethe-Salpeter amplitudes alone, we make the following fundamental approximation: we assume that the two outgoing mesons do not interact with each other, *i.e.* our ansatz relies on the complete neglect of any final state interaction. Then it is allowed to decompose the eight-point Green's function into a product of two four-point Green's functions according to $G^{(8)} \approx G^{(4)} \cdot G^{(4)}$. Considering again only the bound state contributions to four-point Green's functions, we end up with

$$\begin{aligned} \tilde{G}_{\alpha'\alpha'_1, \beta'\beta'_1, \gamma\gamma_1, \gamma'\gamma'_1}^{(8)}(y_1, y_2, z_1, z_2, y'_1, y'_2, z'_1, z'_2) &= - \int d\tilde{P}_2 d\tilde{P}_3 \chi_{\gamma'\beta'}^{P_2}(z_2, y_2) \chi_{\alpha'\gamma}^{P_3}(y_1, z_1) \bar{\chi}_{\beta'_1\gamma'_1}^{P_2}(z'_2, y'_2) \bar{\chi}_{\gamma_1\alpha'_1}^{P_3}(y'_1, z'_1). \end{aligned} \quad (15)$$

Inserting $\tilde{G}^{(4)}$ and $\tilde{G}^{(8)}$ into the defining equation for the irreducible interaction kernel $K^{(6)}$, see eq. (12), we find the following result for the bound state contributions to the six-point Green's function:

$$\begin{aligned} \tilde{G}_{\alpha\alpha', \beta\beta', \gamma\gamma'}^{(6)}(x_1, x_2, y_1, y_2, z_1, z_2) &:= \int d\tilde{P}_1 d\tilde{P}_2 d\tilde{P}_3 \int d^4x'_1 d^4x'_2 d^4y'_1 d^4y'_2 d^4z'_1 d^4z'_2 \\ &\times \chi_{\gamma'\beta'}^{P_2}(z_2, y_2) \chi_{\alpha'\gamma}^{P_3}(y_1, z_1) \bar{\chi}_{\beta'_1\gamma'_1}^{P_2}(z'_2, y'_2) \bar{\chi}_{\gamma_1\alpha'_1}^{P_3}(y'_1, z'_1) \\ &\times K_{\alpha_1\alpha'_1, \beta_1\beta'_1, \gamma_1\gamma'_1}^{(6)}(x'_1, x'_2, y'_1, y'_2, z'_1, z'_2) \chi_{\alpha_1\beta_1}^{P_1}(x'_1, x'_2) \bar{\chi}_{\beta\alpha}^{P_1}(x_1, x_2). \end{aligned} \quad (16)$$

This expression describes the decay of one initial meson into two non-interacting mesons; we will now use it to connect the S -matrix element with the irreducible kernel $K^{(6)}$.

3.2 The S -Matrix Element

The S -matrix operator transforms free states at time $t = -\infty$ into free states at time $t = +\infty$. In terms of a given interaction Lagrangian \mathcal{L}_I , the S -matrix element $S_{P_1 \rightarrow P_2 P_3}$ for an initial meson with momentum P_1

decaying into two outgoing mesons with momenta P_2 and P_3 can be written as

$$S_{P_1 \rightarrow P_2 P_3} = \left\langle P_2 P_3 \left| \sum_{k=0}^{\infty} \frac{i^k}{k!} \int d^4 y_1 \cdots d^4 y_k \mathsf{T} \mathcal{L}_I(y_1) \cdots \mathcal{L}_I(y_k) \right| P_1 \right\rangle. \quad (17)$$

Here, all fields within \mathcal{L}_I are taken as free fields and in normal order. The contribution of this matrix element to the full six-point Green's function $G^{(6)}$ defined in eq. (9) is given by the expression

$$\begin{aligned} \tilde{G}_{\alpha\alpha',\beta\beta',\gamma\gamma'}^{(6)}(x_1, x_2, y_1, y_2, z_1, z_2) &= \int d\tilde{P}_1 d\tilde{P}_2 d\tilde{P}_3 \langle 0 | \mathsf{T} \Psi_{\alpha'}(y_1) \bar{\Psi}_{\beta'}(y_2) \Psi_{\gamma'}(z_2) \bar{\Psi}_{\gamma}(z_1) | P_2 P_3 \rangle \\ &\times \left\langle P_2 P_3 \left| \sum_{k=0}^{\infty} \frac{i^k}{k!} \int d^4 y_1 \cdots d^4 y_k \mathsf{T} \mathcal{L}_I(y_1) \cdots \mathcal{L}_I(y_k) \right| P_1 \right\rangle \\ &\times \langle P_1 | \mathsf{T} \Psi_{\beta}(x_2) \bar{\Psi}_{\alpha}(x_1) | 0 \rangle \end{aligned} \quad (18)$$

where now all fields are free fields taken at $x_1^0, x_2^0 \rightarrow -\infty$ and $y_1^0, y_2^0, z_1^0, z_2^0 \rightarrow +\infty$. As the state $|P_2 P_3\rangle$ is a product of two non-interacting meson states, *i.e.* $|P_2 P_3\rangle = |P_2\rangle |P_3\rangle$, the field operators with the quantum numbers α', γ act (by convention) only on the state $|P_3\rangle$ and the field operators labeled with β', γ' act only on the state $|P_2\rangle$. Thus we can write

$$\langle 0 | \mathsf{T} \Psi_{\alpha'}(y_1) \bar{\Psi}_{\beta'}(y_2) \Psi_{\gamma'}(z_2) \bar{\Psi}_{\gamma}(z_1) | P_2 P_3 \rangle = -\chi_{\alpha'\gamma}^{P_3}(y_1, z_1) \chi_{\gamma'\beta'}^{P_2}(z_2, y_2) \quad (19)$$

and therefore eq. (18) becomes

$$\tilde{G}_{\alpha\alpha',\beta\beta',\gamma\gamma'}^{(6)}(x_1, x_2, y_1, y_2, z_1, z_2) = \int d\tilde{P}_1 d\tilde{P}_2 d\tilde{P}_3 \chi_{\gamma'\beta'}^{P_2}(z_2, y_2) \chi_{\alpha'\gamma}^{P_3}(y_1, z_1) S_{P_1 \rightarrow P_2 P_3} \bar{\chi}_{\beta\alpha}^{P_1}(x_2, x_1). \quad (20)$$

By comparing this expression with eq. (16), the connection between the S -matrix element $S_{P_1 \rightarrow P_2 P_3}$, the irreducible kernel $K^{(6)}$ and the Bethe-Salpeter amplitudes of the three mesons can be written according to

$$\begin{aligned} S_{P_1 \rightarrow P_2 P_3} &= - \int d^4 x'_1 d^4 x'_2 d^4 y'_1 d^4 y'_2 d^4 z'_1 d^4 z'_2 \\ &\times \mathsf{tr} \left[\bar{\chi}^{P_2}(z'_2, y'_2) \bar{\chi}^{P_3}(y'_1, z'_1) K^{(6)}(x'_1, x'_2, y'_1, y'_2, z'_1, z'_2) \chi^{P_1}(x'_1, x'_2) \right]; \end{aligned} \quad (21)$$

here, we have abbreviated the full contraction of all multi-indices by the trace symbol tr . In the following, we will specify the particular interactions summarized in the six-point kernel $K^{(6)}$.

3.3 Approximation of the Interaction Kernel

The uncontracted term of the 't Hooft Lagrangian $\Delta\mathcal{L}^{\text{eff}}$ (see appendix B) yields an explicit expression for an effective six-quark interaction Lagrangian $\mathcal{L}_I = \mathcal{L}^{(3)}$ given in eq. (37). Up to the first order in the instanton coupling $g_{\text{eff}}^{(3)}$, the S -matrix element $S_{P_1 \rightarrow P_2 P_3}$ in eq. (17) consists of two terms:

$$S_{P_1 \rightarrow P_2 P_3} = \langle P_2 P_3 | P_1 \rangle + \langle P_2 P_3 | i \int d^4 y \mathcal{L}^{(3)}(y) | P_1 \rangle + \mathcal{O}(g_{\text{eff}}^{(3)})^2. \quad (22)$$

The first term is of order $\mathcal{O}(1)$ in the coupling of the six-quark interaction, *i.e.* the 't Hooft three-body interaction via $\mathcal{L}^{(3)}$ is absent and the decay passes exclusively over the propagation of non-interacting quarks. The second term is of order $\mathcal{O}(g_{\text{eff}}^{(3)})$, *i.e.* the quarks of the three mesons once interact via $\mathcal{L}^{(3)}$.

To find the corresponding interaction kernel, we consider the six-point Green's function, see eq. (9), up to this order; it thus can be decomposed into two terms according to $G^{(6)} = G_0^{(6)} + G_1^{(6)} + \dots$. In the following, the (anti-)quark fields $\Psi(\bar{\Psi})$ are free fields in the sense that they are out of the interaction region. By using Wick's theorem and after inserting several δ -distributions, we get for the lowest-order term the expression

$$\begin{aligned} G_0^{(6)}_{\alpha\alpha',\beta\beta',\gamma\gamma'}(x_1, x_2, y_1, y_2, z_1, z_2) &:= \langle 0 | \mathsf{T} \Psi_{\alpha'}(y_1) \bar{\Psi}_{\beta'}(y_2) \Psi_{\gamma'}(z_2) \bar{\Psi}_{\gamma}(z_1) \Psi_{\beta}(x_2) \bar{\Psi}_{\alpha}(x_1) | 0 \rangle \\ &= - \int d^4 x'_1 d^4 x'_2 d^4 y'_1 d^4 y'_2 d^4 z'_1 d^4 z'_2 \delta_{\alpha_1\alpha'} \delta_{\beta_1\beta'} \delta_{\gamma_1\gamma'} \\ &\times \delta(x'_1 - y'_1) \delta(x'_2 - y'_2) \delta(z'_1 - z'_2) \delta(y'_1 - y_1) \delta(y'_2 - y_2) \delta(z'_2 - z_2) \\ &\times \langle 0 | \mathsf{T} \Psi_{\alpha_1}(x'_1) \bar{\Psi}_{\alpha}(x_1) | 0 \rangle \langle 0 | \mathsf{T} \Psi_{\beta}(x_2) \bar{\Psi}_{\beta_1}(x'_2) | 0 \rangle \langle 0 | \mathsf{T} \Psi_{\gamma_1}(z'_1) \bar{\Psi}_{\gamma}(z_1) | 0 \rangle \\ &+ \text{crossed term} . \end{aligned}$$

The crossed term follows from the first term by exchanging $(z_2, \gamma') \longleftrightarrow (y_1, \alpha')$ and $(z_1, \gamma) \longleftrightarrow (y_2, \beta')$; see also figs. 1 and 2.

Now we approximate the full Feynman propagators by the free propagators with effective constituent quark masses, consistent with the approximation done in the Bethe-Salpeter equation (see section 2.1). In coordinate space, they satisfy the relations

$$(i \not{\partial}_x - m)_{\alpha\alpha'} S_{\alpha'\beta}^F(x, x') = +i\delta(x - x')\delta_{\alpha\beta} \quad (23)$$

$$\text{and } S_{\alpha\alpha'}^F(x, x')(i \not{\partial}_{x'} + m)_{\alpha'\beta} = -i\delta(x - x')\delta_{\alpha\beta} . \quad (24)$$

Inserting these relations into eq. (23) and using $S_{\alpha\alpha'}^F(x, x') := \langle 0 | \mathcal{T} \Psi_\alpha(x) \bar{\Psi}_{\alpha'}(x') | 0 \rangle$, we get for the quark loop part $G_0^{(6)}$ of the six-point Green's function the following result:

$$\begin{aligned} G_0^{(6)}_{\alpha\alpha', \beta\beta', \gamma\gamma'}(x_1, x_2, y_1, y_2, z_1, z_2) &= -i \int d^4 x'_1 d^4 x'_2 d^4 y'_1 d^4 y'_2 d^4 z'_1 d^4 z'_2 \\ &\times \left[S_1^F(y_1, y'_1) (-i \not{\partial}_{y'_1} - m_1) S_1^F(x'_1, x_1) \right]_{\alpha'\alpha} \delta(x'_1 - y'_1) \\ &\times \left[S_2^F(x_2, x'_2) (+i \not{\partial}_{y'_2} - m_2) S_2^F(y'_2, y_2) \right]_{\beta\beta'} \delta(x'_2 - y'_2) \\ &\times \left[S_3^F(z_2, z'_2) (-i \not{\partial}_{z'_2} - m_3) S_3^F(z'_1, z_1) \right]_{\gamma'\gamma} \delta(z'_2 - z'_1) \\ &+ \text{crossed term} . \end{aligned} \quad (25)$$

Here, the constituent quark masses of the incoming quark and anti-quark are denoted by m_1 and m_2 , respectively; the constituent quark mass of the third quark is labeled by m_3 .

Now we want to determine the irreducible six-point kernel $K^{(6)}$ introduced in eq. (12). In this defining equation, we now approximate the four-point Green's function by its free part and adopt $G_{\alpha_1\alpha, \beta_1\beta}^{(4)}(x'_1, x'_2, x_1, x_2) \approx S_{\alpha_1\alpha}^F(x'_1, x_1) S_{\beta\beta_1}^F(x_2, x'_2)$. Accordingly, we insert this four-point Green's function in the decomposition $G^{(8)} \approx G^{(4)} \cdot G^{(4)}$ of the eight-point Green's function since we neglect all effects originating in final state interactions of the outgoing mesons. With this assumptions, we can read off the lowest-order part of the six-point kernel defined in eq. (12) as follows:

$$\begin{aligned} K_0^{(6)}_{\alpha_1\alpha'_1, \beta_1\beta'_1, \gamma_1\gamma'_1}(x'_1, x'_2, y'_1, y'_2, z'_1, z'_2) &= -i \delta(x'_1 - y'_1) \delta(x'_2 - y'_2) \delta(z'_2 - z'_1) \\ &\times (-i \not{\partial}_{y'_1} - m_1)_{\alpha'_1\alpha_1} (+i \not{\partial}_{y'_2} - m_2)_{\beta_1\beta'_1} (-i \not{\partial}_{z'_2} - m_3)_{\gamma'_1\gamma_1} \\ &+ \text{crossed term} . \end{aligned} \quad (26)$$

The next term $G_1^{(6)}$ in the six-point Green's function is of order $\mathcal{O}(g_{\text{eff}}^{(3)})$ in the instanton-induced interaction; starting with its definition

$$\begin{aligned} G_1^{(6)}_{\alpha\alpha', \beta\beta', \gamma\gamma'}(x_1, x_2, y_1, y_2, z_1, z_2) &= i \int d^4 y \langle 0 | \mathcal{T} \Psi_{\alpha'}(y_1) \bar{\Psi}_{\beta'}(y_2) \Psi_{\gamma'}(z_2) \bar{\Psi}_{\gamma}(z_1) \Psi_{\beta}(x_2) \bar{\Psi}_{\alpha}(x_1) \mathcal{L}^{(3)}(y) | 0 \rangle , \end{aligned} \quad (27)$$

it can be derived in analogy to the pure quark loop part. Using the anti-symmetry of the operator \mathcal{O}^{FSC} defined in eq. (40) in appendix B.2, the result for the interaction kernel reads

$$\begin{aligned} K_1^{(6)}_{\alpha_1\alpha'_1, \beta_1\beta'_1, \gamma_1\gamma'_1}(x'_1, x'_2, y'_1, y'_2, z'_1, z'_2) &= -i 36 g_{\text{eff}}^{(3)} \cdot \mathcal{O}_{\beta_1\alpha'_1\gamma'_1\alpha_1\gamma_1\beta'_1}^{FSC} \\ &\times \int d^4 y \delta(x'_1 - y) \delta(x'_2 - y) \delta(y'_1 - y) \delta(y'_2 - y) \delta(z'_1 - y) \delta(z'_2 - y) . \end{aligned} \quad (28)$$

where we have inserted the explicit expression for the instanton-induced interaction Lagrangian $\mathcal{L}^{(3)}$ (see appendix B); the numerical factor arises from 36 identical terms found by performing Wick's theorem to $G_1^{(6)}$. By comparison of $G^{(6)} = G_0^{(6)} + G_1^{(6)}$ up to order $\mathcal{O}(g_{\text{eff}}^{(3)})$ with the defining equation (12) for the irreducible interaction kernel, we thus find $K^{(6)} = K_0^{(6)} + K_1^{(6)}$ in the same approximation.

3.4 The Transition Matrix Element

The S –matrix element as given in eq. (21) up to first order in the three–body coupling constant $g_{\text{eff}}^{(3)}$ follows from insertion of the irreducible six–point kernel in the same order. To obtain a more compact notation, we relabel some integration variables, use again the trace symbol tr for the contraction of all multi–indices and finally find

$$\begin{aligned} S_{P_1 \rightarrow P_2 P_3} &= i \int d^4x d^4y d^4z \text{ tr} \left[\bar{\chi}^{P_2}(z, y) (i \not{\partial}_z + m_3) \bar{\chi}^{P_3}(x, z) (i \not{\partial}_x + m_1) \chi^{P_1}(x, y) (i \not{\partial}_y - m_2) \right] \\ &+ i \int d^4x d^4y d^4z \text{ tr} \left[\bar{\chi}^{P_3}(z, x) (i \not{\partial}_z + m_3) \bar{\chi}^{P_2}(y, z) (i \not{\partial}_y + m_1) \chi^{P_1}(y, x) (i \not{\partial}_x - m_2) \right] \\ &+ i 36 g_{\text{eff}}^{(3)} \int d^4y \text{ tr} \left[\mathcal{O}^{FSC} (\bar{\chi}^{P_3}(y, y) \otimes \bar{\chi}^{P_2}(y, y) \otimes \chi^{P_1}(y, y)) \right]. \end{aligned} \quad (29)$$

We now perform a Fourier transformation into momentum space and use the well–known general relation between the transition operator T and the S –matrix operator given by $S_{fi} = \delta_{fi} + i(2\pi)^4 \delta(P_f - P_i) \langle f | T | i \rangle$ with $|i\rangle$ and $|f\rangle$ initial and final state, respectively. Finally, we find the following transition amplitude up to first order in the coupling of 't Hooft's instanton–induced three–body interaction:

$$T_{P_1 \rightarrow P_2 P_3} = \langle P_2 P_3 | T | P_1 \rangle = T_{P_1 \rightarrow P_2 P_3}^{\text{loop}} + T_{P_1 \rightarrow P_2 P_3}^{\text{'t Hooft}} + \mathcal{O}((g_{\text{eff}}^{(3)})^2) \quad (30)$$

$$\begin{aligned} \text{with } T_{P_1 \rightarrow P_2 P_3}^{\text{loop}} &:= \int \frac{d^4p}{(2\pi)^4} \text{ tr} \left[\bar{\Gamma}^{P_2}(p - \frac{P_3}{2}) S_3^F(\frac{P_2 - P_3}{2} + p) \bar{\Gamma}^{P_3}(p + \frac{P_2}{2}) S_1^F(\frac{P_1}{2} + p) \Gamma^{P_1}(p) S_2^F(-\frac{P_1}{2} + p) \right] \\ &+ \int \frac{d^4p}{(2\pi)^4} \text{ tr} \left[\bar{\Gamma}^{P_3}(p - \frac{P_2}{2}) S_3^F(\frac{P_3 - P_2}{2} + p) \bar{\Gamma}^{P_2}(p + \frac{P_3}{2}) S_1^F(\frac{P_1}{2} + p) \Gamma^{P_1}(p) S_2^F(-\frac{P_1}{2} + p) \right] \\ \text{and } T_{P_1 \rightarrow P_2 P_3}^{\text{'t Hooft}} &:= 36 g_{\text{eff}}^{(3)} \text{ tr} \left[\mathcal{O}^{FSC} \left(\bigotimes_{i=1}^3 \int \frac{d^4p_i}{(2\pi)^4} \mathcal{X}_i^{P_i}(p_i) \right) \right] . \end{aligned}$$

The trace runs over colour, flavour and spin indices; by definition, momentum conservation is fulfilled, *i.e.* $P_1 = P_2 + P_3$ holds. In the quark loop part, we have expressed the Bethe–Salpeter amplitudes by the corresponding vertex functions according to their definition given in section 2.1. Note that we have introduced $\mathcal{X}_1 = \chi$ and $\mathcal{X}_2 = \mathcal{X}_3 = \bar{\chi}$ in order to distinguish properly the Bethe–Salpeter amplitude and its adjoint.

3.5 Calculation of the Decay Width

After we have derived the transition matrix element $T_{P_1 \rightarrow P_2 P_3}$ for the mesonic strong decay $\mathcal{M}_1 \rightarrow \mathcal{M}_2 \mathcal{M}_3$, we will finally give the standard formula for the calculation of the partial decay width:

$$\Gamma_{\mathcal{M}_1 \rightarrow \mathcal{M}_2 \mathcal{M}_3} = \frac{k}{8\pi M_1^2} \sum_{m_1} \frac{1}{2J_1 + 1} \sum_{m_2, m_3} \left| \langle P_2 m_2 P_3 m_3 | T | P_1 m_1 \rangle \right|^2 ; \quad (31)$$

here, $k^2 = (P_2^0)^2 - M_2^2 = (P_3^0)^2 - M_3^2$ in the rest frame of the incoming meson (*i.e.* $P_1 = \begin{pmatrix} M_1 \\ 0 \end{pmatrix}$) is a kinematical factor, $m_i := m_{J_i}$ ($i = 1, 2, 3$) are the magnetic quantum numbers and $P_1 = P_2 + P_3$ holds due to four–momentum conservation. In appendix A, we comment on the flavour matrix element and on the particular factors corresponding to the charge multiplicities.

In fig. 2, we summarize the results of this section in a diagrammatical representation. As we have shown in the framework of the Mandelstam formalism, the pure quark loop term contributes to all strong two–body decays. In contrast to this general mechanism, the instanton–induced decay via the three–body vertex of the 't Hooft Lagrangian only takes place if all mesons in the decay are either of scalar or pseudoscalar type, *i.e.* if $J_i = 0$ ($i = 1, 2, 3$) holds. In this case, we expect the interference between the quark loop terms and the instanton–induced contributions to modify the results on the strong decay widths in our calculation in a characteristical fashion.

Let us make a final remark before we study in detail the numerical results concerning the strong meson decays. It is obvious from fig. 2 that the quark loop part satisfies the well–known Zweig rule (or OZI rule). For the instanton–induced decay mechanism, the situation is different if and only if a flavour singlet participates in

the decay under consideration. In order to see this, we write down the explicit flavour dependence of this interaction (see also [13, 31, 32]) as

$$\text{tr} \left[\mathcal{P}_1^F (\Lambda^{\mathcal{M}_1} \otimes \Lambda^{\mathcal{M}_2} \otimes \Lambda^{\mathcal{M}_3}) \right] = \frac{1}{6} \epsilon^{ijk} \epsilon^{i'j'k'} \Lambda_{ii'}^{\mathcal{M}_1} \Lambda_{jj'}^{\mathcal{M}_2} \Lambda_{kk'}^{\mathcal{M}_3}. \quad (32)$$

Here, $\Lambda^{\mathcal{M}_i}$ ($i = 1, 2, 3$) is the flavour part of Bethe-Salpeter amplitude for the meson \mathcal{M}_i and the whole expression originates in the term $T_{P_1 \rightarrow P_2 P_3}^{'t \text{ Hooft}}$ of eq. (30). Note that \mathcal{P}_1^F projects onto singlet states in flavour space; this projector is part of the general operator \mathcal{O}^{FSC} defined in eq. (40) in appendix B.2. The expression in eq. (32) shows that the instanton-induced six-quark interaction is completely antisymmetric in flavour space. With the help of the Cayley-Hamilton theorem, the flavour dependence can be rewritten as

$$\begin{aligned} \text{tr} \left[\mathcal{P}_1^F (\Lambda^{\mathcal{M}_1} \otimes \Lambda^{\mathcal{M}_2} \otimes \Lambda^{\mathcal{M}_3}) \right] &= \frac{1}{6} \text{tr} \left[\Lambda^{\mathcal{M}_1} \Lambda^{\mathcal{M}_2} \Lambda^{\mathcal{M}_3} + \Lambda^{\mathcal{M}_1} \Lambda^{\mathcal{M}_3} \Lambda^{\mathcal{M}_2} \right] \\ &- \frac{1}{6} \left(\text{tr} \left[\Lambda^{\mathcal{M}_1} \right] \text{tr} \left[\hat{\Lambda}^{\mathcal{M}_2} \hat{\Lambda}^{\mathcal{M}_3} \right] + \text{cycl. perm.} \right) \end{aligned} \quad (33)$$

where $\hat{\Lambda}^{\mathcal{M}_i}$ denotes the traceless part of $\Lambda^{\mathcal{M}_i}$ (see [13, 31]). Here, the first term has the flavour dependence of usual quark loop diagrams — see fig. (2) — such that this interaction gives an additional contribution to the conventional Zweig rule allowed transitions for decays involving only $J_i = 0$ mesons ($i = 1, 2, 3$). The flavour dependence of the second term leads to a minimal violation of the OZI rule: only if $\text{tr} [\Lambda^{\mathcal{M}_i}]$ does not vanish, *i.e.* if and only if a flavour singlet participates, there is an additional contribution to the conventional decay mechanism beyond the Zweig rule allowed processes.

4 Results and Discussion

As we have already mentioned in section 2.2, we have calculated the masses of light mesons in two different parameter sets for the confinement force (see [11, 12]). Both models yielded an excellent description of the experimental ground state Regge trajectories while the masses of the pseudoscalar ground state nonet were very well described by using 't Hooft's force as an additional residual interaction. However, we found the radial excitation spectrum as well as the complete scalar meson spectrum considerably different in both models. Especially the latter sector needs further investigations beyond purely spectroscopical considerations in order to understand the nature of the scalar mesons. The study of hadronic decays presented in this contribution may help for a more serious interpretation of these mesons. However, the calculation of strong decay widths for the complete resonance spectrum is of course first of all important in its own right.

In this publication, we study strong two-body decays under the assumption that any final state interaction can be neglected. In this approximation, the transition matrix element for the decay of one initial meson \mathcal{M}_1 with four momentum P_1 into two outgoing mesons \mathcal{M}_2 and \mathcal{M}_3 with four momenta P_2, P_3 (for the bound states masses, $M_i^2 = P_i^2$ holds) is evaluated up to first order in the effective coupling of the instanton induced three-body interaction $\mathcal{L}^{(3)}$, see eqs. (22) and (30).

In the lowest order term, the instanton-induced interaction is absent and the decay passes over the propagation of non-interacting quarks forming a simple loop. These transitions are Zweig rule allowed and they always contribute, independent of the quantum numbers of the three mesons that are involved in the decay under consideration. The next term in the transition matrix element of eq. (30) is of order $\mathcal{O}(g_{\text{eff}}^{(3)})$, *i.e.* the quarks of the three mesons once interact via the instanton-induced interaction described by $\mathcal{L}^{(3)}$ (see also appendix B.2). These transitions only contribute if all three mesons have vanishing total angular momentum $J_i = 0$ ($i = 1, 2, 3$) such that the decays of other than scalar and pseudoscalar mesons are not influenced by this interaction. The transition amplitude generated by $\mathcal{L}^{(3)}$ contains a Zweig rule violating part if a flavour singlet meson is involved in the decay under consideration.³

At this point, a short remark on our selection of the decays in our following discussion is in order.⁴ In general, we only quote our results on particular decay widths if it can either be compared with an experimental value

³This hierarchy of decay mechanisms in our approach suggests a clear indication whether or not the instanton-induced effects contribute to a specific decay. In all tables summarizing our numerical results, we thus indicate by the symbol “•” in the column “III” if the three-body 't Hooft interaction plays a role, *i.e.* if we expect an interference of the amplitudes originating both in quark loop diagrams and instanton-induced decay mechanisms. Furthermore, we point out by an additional symbol “•” in the column “ZRV” whether Zweig rule violating processes contribute to the decay width or not; as we have shown above, effects beyond the OZI rule allowed diagrams are expected if isoscalar mesons participate the instanton-induced decay process.

⁴Note that we denote the final state “ $K\bar{K} + \text{c.c.}$ ” by “ KK ”; analogously, we abbreviate the “ $K\bar{K}^* + \text{c.c.}$ ” final state with “ KK^* ” for simplicity.

or with data obtained in the framework of the 3P_0 model. For the latter reference, we usually quote the results of T. Barnes *et al.* published in refs. [6, 7]; we refer to R. Bonnaz and B. Silvestre-Brac with respect to the decays of non- $n\bar{n}$ mesons (see [8]).⁵

Let us give also a brief comment on two recently published works: In [38], strong decays of light vector mesons are studied within a covariant approach combining Bethe-Salpeter and Dyson-Schwinger equations. For the related coupling constants the authors find good agreement with the experimental results; note that only quark loops contribute to their calculated widths. A further interesting review (see [39]) describes 3P_0 model results for strange quarkonia. As most of the strong decay widths in this paper are parametrized in terms of a singlet-triplet mixing angle, which is not uniquely fixed *a priori* by experiment, we will not discuss their results in more detail.

4.1 Fixing the Three-Body Coupling Constant

Before we discuss the numerical results for the various decay widths, we shall briefly comment on our choice for the value of the coupling constant $g_{\text{eff}}^{(3)}$ which governs the strength of the instanton-induced six-quark vertex. As we show in fig. 3(a), we fix this free parameter at the width for the decay $K_0^*(1430) \rightarrow K\pi$, namely $\Gamma_{\text{exp}} = 274 \pm 37$ MeV. Compared to other decays in which all participating mesons have total angular momentum $J_i = 0$, this width is quite well-known experimentally which suggests to fix the free parameter by this number. However, the uncertainty is still large such that we cannot be sure to have optimally fixed $g_{\text{eff}}^{(3)}$. Moreover, the parameter set used in this work has the special feature that — at a first glance — underestimates the masses of the scalar bound states such as the K_0^* mesons; note that nevertheless our results agree excellently with the K -matrix analyses done by V. V. Anisovich and co-workers (see [33] as well as our discussion in [12]). Thus, the particular phase space factor in the decay $K_0^*(1430) \rightarrow K\pi$ is not well described in our model as the scalar kaon mass is roughly 200 MeV smaller than compared to the standard value of the PDG (see [14]). We have however decided to fix the 't Hooft coupling $g_{\text{eff}}^{(3)}$ at the experimental value for the decay $K_0^*(1430) \rightarrow K\pi$. Our approach is justified by the observation that our choice simultaneously allows for a correct description of the decay $K_0^*(1950) \rightarrow K\pi$, see fig. 3(b). In particular, it is impressive to see how the instanton-induced contribution to the decay widths in these examples raises dramatically the pure quark loop contribution of only a few MeV up to the experimental values of several hundred MeV.

4.2 Decays of ρ_J Mesons

In tab. 3, we have listed our result concerning the strong two-body decays of isovector ρ_J mesons; in particular, we study the $\rho(770)$, $\rho(1450)$, $\rho(1700)$ and $\rho_3(1690)$. We shall note that the radial excitation pattern in this sector is slightly different to what is usually assumed for the ρ mesons: while the masses of the $\rho(770)$ and $\rho(1450)$ are quite well described in our approach, we underestimate the $\rho(1700)$ mass by roughly ≈ 200 MeV (see [11]). Note that our calculation implies that the $\rho(770)$ and $\rho(1700)$ are dominantly S -wave mesons while the $\rho(1450)$ and $\rho_3(1690)$ are dominantly D -wave mesons (see appendix of ref. [34] for comparison).

Comparing our result for the $\rho(770) \rightarrow \pi\pi$ decay with experiment and the 3P_0 model, we see that both theoretical approaches underestimate the partial decay width $\Gamma_{\text{exp}} \approx 150$ MeV such that the strong two-body decay mode alone cannot saturate the total $\rho(770)$ width in both approaches. This is a first hint that the neglect of final-state interaction in our ansatz might spoil our results in certain sectors although we use a completely relativistic formula for the calculation of the quark loop diagram.

The various decay modes of the $\rho(1450)$ are in general very small in our approach compared to the 3P_0 model. However, a look at the experimental limits in this sector leads to the conclusion that our results for the decays $\rho(1450) \rightarrow \omega\pi/\rho\eta/KK$ are at least consistent with these rough limits while the results of ref. [7] strongly overestimate the related partial widths. For the $\rho(1700)$, an analogous statement holds: the widths calculated in the framework of our model are very small compared to the 3P_0 — however, they do not contradict the experimental limit *e.g.* for the decay $\rho(1700) \rightarrow \rho\eta$ with $\Gamma_{\text{exp}} < 9.6$ MeV. For both radial ρ excitations, the total experimental width is again significantly larger than the sum of the partial width calculated in our approach.

For the strong decays of the $\rho_3(1690)$, we find that especially the $\pi\pi$ partial width is significantly too small. This observation might be related to the fact that the description of the pion in the framework of our model is not overall satisfying; as we have already noted in ref. [11], the instantaneous approximation seems to be

⁵To be precise, we refer to their parameter set labeled ‘‘NRAL’’ with a momentum-dependent 3P_0 -vertex including instanton-induced as well as tensor-force effects. For outgoing mesons with broad widths (> 50 MeV), the authors introduced a modified mechanism for the description of this situation; note that this approach has severe problems due to the inherent violation of Galilei invariance of the 3P_0 model.

not well suited for a deeply bound state such as the π meson. For the strong decays, the related wave function deformation leads to a general underestimation of partial widths if one or two pions are observed in the final state. As our calculated widths for the decays $\rho_3(1690) \rightarrow \rho\eta/KK$ are plausible compared to experiment as well as to the 3P_0 model result, this problem seems to be restricted to pionic final states at the moment. In fact, the large $\rho_3(1690) \rightarrow \rho\rho$ width in our framework is comparable with the 3P_0 model.

4.3 Decays of π_J Mesons

The results of the strong π_J meson decay are presented in tab. 4; let us note that the masses of the $\pi(1300)$, $\pi(1800)$ and $\pi_2(1670)$ are well described in our model (see [11]).

Again, we find that the calculated widths are significantly smaller than the results of the 3P_0 model but the experimental data are quite poor for the $\pi(1300)$ and $\pi(1800)$ such that a detailed comparison is difficult. We note that we also find small widths for the decays $\pi(1800) \rightarrow \rho\pi/KK^*$ which have not been seen in experiment; here, the approach of ref. [7] seems to overestimate the partial widths.

At this point, a further remark concerning the contributions of 't Hooft's six-quark interaction is in order. As we have denoted it in tab. 4 in the columns "III" and "ZRV", the decays $\pi(1800) \rightarrow f_0(1370)\pi/f_0(1500)\pi/a_0(980)\eta/KK_0^*$ not only include the simple quark loop mechanism but also obtain a significant contribution by the instanton induced interaction. In general, the interference between both terms can either be constructive or destructive. For the pion decays discussed in this section, the interference is destructive and therefore lowers the resulting partial widths compared to the pure quark loop contribution.

Concerning the $\pi_2(1670)$ decays, we still find generally too small widths; at least for the pion-free final state KK^* , we obtain a plausible result. Note that the 3P_0 model gives a vanishing partial width for the $f_0(1370)\pi$ decay mode in contradiction to experiment; also for other final states, the non-relativistic 3P_0 ansatz is less accurate than often claimed.

4.4 Decays of ω_J and ϕ_J Mesons

In tab. 5, we summarize our results for the strong partial decay widths of the isoscalar ω_J and ϕ_J mesons. Their masses are quite well described in our Bethe-Salpeter ansatz; note that — due to the lack of a mixing mechanism for $J \neq 0$ mesons — the ω_J are purely $n\bar{n}$ states while the ϕ_J are purely $s\bar{s}$ states in good agreement with their experimental status. We assume the $\omega(1420)$ to be the second radial $n\bar{n}$ excitation in this sector as this meson is considered as an S -wave state in ref. [7]; analogously, we consider the $\phi(1680)$ to be the second radially excited $s\bar{s}$ state (see also the appendix of ref. [34]).

As we have already observed before, the total widths of the ω_J mesons cannot be saturated by the sum of their two-body strong decay widths alone; although there in fact exist numerous other (pre-dominantly electromagnetic) decay modes (see [14]), this leads again to some inconsistencies between our relativistic quark loop approach and the results of the 3P_0 model.

Unfortunately, we cannot compute the $\phi(1020) \rightarrow KK$ decay due to kinematical reasons: although the calculated masses for the ϕ and the K mesons are accurate up to only $\approx 3\%$, the relation $M_\phi \geq 2M_K$ is missed by a few MeV and thus a calculation of this decay is prohibited. We could of course slightly re-adjust our model parameters (*e.g.* to lower the K mass a little bit); however, we have refrained from such a manipulation as the decay rate is obviously extremely sensible on the precise values of the phase space factor in $\phi(1020) \rightarrow KK$, see also eq. (31). The other partial widths of the $\phi(1020)$ are found to be strictly zero in our model since a $s\bar{s}$ state clearly cannot decay into two $n\bar{n}$ states via a simple quark loop mechanism alone; the non-vanishing experimental widths for $\phi(1020) \rightarrow \pi\pi/\omega\pi$ indicate that additional diagrams beyond lowest order in fact play a role for some decays even if mesons with non-zero total angular momentum are involved in the process. For the decays of the $\phi(1680)$ and $\phi_3(1850)$ into kaon pairs, we find at least plausible results by considering the quark loop contribution; again, the sums of the KK and KK^* decay widths are not sufficient to explain the total decay widths of these mesons.

4.5 Decays of h_J and b_J Mesons

The decay widths of the isoscalar h_J and isovector b_J mesons are summarized in tab. 6. Note that the $n\bar{n}$ states $h_1(1700)/b_1(1700)$ and $h_3(2050)/b_3(2050)$ are not listed by the PARTICLE DATA GROUP (see [14]); however, their (degenerated) masses assumed in the framework of the 3P_0 model in ref. [7] fit excellently to the numerical results of our relativistic quark model (see [11, 34]). Thus, we have decided to list their decay widths although no experimental data concerning their partial widths exist so far.

The $\rho\pi$ decay modes of the h_J mesons are not as dominant in our calculation as they appear in the 3P_0

model. In fact, our calculation yields a larger partial width if the first radial ρ excitation is in the final state. Concerning the vanishing probability of the decays into a $b_1(1235)\pi$ final state, we observe a similarity between our approach and the 3P_0 model. The comparison concerning the other b_J decay modes show that the $\rho\rho$ final state is strongly suppressed in our calculation while — in the framework of the 3P_0 model — it plays a significant role in the $b_1(1700)$ and $b_3(2050)$ decays. We refrain from a further discussion of this sector as there are no reliable experimental data to compare with so far.

4.6 Decays of a_J Mesons

We review our results concerning the a_J strong decays in tab. 7. The masses of these isovector mesons are quite well described as the a_0 masses are only slightly overestimated while the a_J masses for $J \neq 0$ are correctly calculated up to only a few percent in our approach (see [11]); note that this statement also holds for the radial excitations in this sector.

Let us first focus on the strong two-body decays of the $a_0(980)$ and $a_0(1450)$ mesons. The relative strength of the $\eta\pi$ and KK decay modes are well reproduced for the a_0 ground state. For the radial excitation, the pattern is again quite plausible: the decay widths add up to ≈ 100 MeV compared to only ≈ 10 MeV in the 3P_0 model which strongly underestimates the experimentally determined total decay width. In fig. 4, we show how the instanton-induced six-quark interaction significantly lifts the $\eta\pi$ partial width of the $a_0(980)$ and $a_0(1450)$ mesons; without this contribution (*i.e.* for $g_{\text{eff}}^{(3)} = 0$), the quark loop diagram alone would in fact give results of only a few MeV as predicted by the 3P_0 model. We consider the interplay between the quark loop and the instanton-induced contribution to these decay widths as an impressive feature of our ansatz that includes diagrams beyond lowest order. The interference of OZI allowed and OZI forbidden contributions can clearly be studied in fig. 4; obviously, the Zweig rule violating processes are important for the understanding of these decays. In this example, the relative sign between both parts leads to a destructive interference finally yielding partial widths in the correct order of magnitude. This underlines our introductory statement that the instanton-induced mechanism plays a crucial role in the description of scalar meson decays.

The lack of diagrams induced by 't Hooft instanton force is visible in our results for the a_1 mesons. They are smaller by an order of magnitude compared to the non-relativistic 3P_0 model; we thus find again that the pure quark loop calculations underestimate the partial widths in the presence of one or two pions in the final state. However, the decays of the $a_2(1320)$ are plausibly described in our relativistic approach compared to the 3P_0 model as well as to experiment. The accuracy of our results is not satisfying; nevertheless, the numbers in tab. 7 clearly show that an approximative agreement with the experimental data for the $a_2(1320)$ partial widths can be achieved without any re-adjustment of our fundamental model parameters.

4.7 Decays of f_J Mesons

The strong decays of the isoscalar f_J mesons are particularly interesting as they might allow for an identification of the possible non- $q\bar{q}$ nature of certain mesons in this sector. In tabs. 8 and 9, we summarize our results concerning the f_J mesons and compare them with experimental data and (rare) results of the 3P_0 model. Note that the masses of these mesons are correctly determined within our approach up to only a few percent (see [11, 34]).

Let us first consider the decays $f_0 \rightarrow \pi\pi$ for the ground state ($M_{f_0} \approx 400 \dots 1200$ MeV ≈ 665 MeV), the first ($M_{f_0} \approx 1370$ MeV) and the second ($M_{f_0} \approx 1500$ MeV) radial excitation. We have plotted the partial decay widths with respect to their dependence on the six-quark coupling $g_{\text{eff}}^{(3)}$ of 't Hooft's force in fig. 5. As all mesons in these decays have total angular momentum $J = 0$, the instanton-induced interaction provides an additional contribution to the decay widths beyond the lowest order quark loop diagrams. Moreover, we observe Zweig rule violating amplitudes in these decays as the f_0 mesons are isoscalar (see section 3.5 for comparison). The widths based on OZI allowed processes and OZI forbidden processes are indicated in fig. 5; the fat solid line in these plots denote the total partial width for $f_0 \rightarrow \pi\pi$ produced by the interference of the underlying mechanisms.

At this point, we want to comment on the frequently discussed considerations of the scalar nonet in standard (mainly nonrelativistic) quark models: Due to the suppression of the decay mode $f_0(1500) \rightarrow K\bar{K}$, the $f_0(1500)$ should be assigned to a dominantly $\bar{n}n$ -state rather than to a dominantly $\bar{s}s$ -state. Then this resonance may be viewed as the isoscalar partner of the $a_0(1450)$ and $K_0^*(1430)$. Whereas the observed widths for the latter resonances (~ 300 MeV) can be well reproduced in the standard quark models, the same models yield $\Gamma(f_0(1500)) > 500$ MeV in clear contradiction to experiment. From this point of view the experimental width of the $f_0(1500)$ indeed seems to be “unnaturally small”. However, these arguments are completely wrong if Zweig rule violating forces are taken into account; merely, the conventional conclusion

concerning the flavour contents of resonances, which may be roughly formulated as “dominant $\pi\pi$ decay mode indicates large nonstrange contents in the decaying resonance” and “dominant $K\bar{K}$ decay mode indicates large strange contents in the decaying resonance”, is certainly not true for mesons that can decay via the instanton induced six-quark interaction via a Zweig rule violating process.

In fig. 5(a), the decay $f_0(400\dots 1200) \rightarrow \pi\pi$ is plotted; obviously, the interference between OZI allowed processes and OZI forbidden processes is destructive. The Zweig rule violating width is huge at $g_{\text{eff}}^{(3)} = 71.4 \text{ GeV}^{-5}$; due to the destructive interference of the different amplitudes, the resulting partial width is however reduced to only 297 MeV which is quite realistic for this decay mode. Note that the pure quark loop contribution in this example is only ≈ 40 MeV which would clearly underestimate the $\pi\pi$ width of the σ meson; again, we thus see the interesting influence of the additional instanton-induced contribution to the partial width. The analogue plots for the decays $f_0(1370) \rightarrow \pi\pi$ and $f_0(1500) \rightarrow \pi\pi$ are given in figs. 5(b) and 5(c). For the $f_0(1370)$ decay, we observe a constructive interference of the OZI allowed and OZI forbidden amplitudes lifting the partial width to 477 MeV which is comparable to the 3P_0 model with 271 MeV (see [6]). However, the experimental width given in ref. [15] is significantly smaller, namely $\Gamma_{\text{exp}} = 21.7 \pm 9.9$ MeV. In the CRYSTAL BARREL experiment presented in this publication, the $f_0(1370)$ dominantly decays into its $\sigma\sigma$ mode. Unfortunately, we cannot compute this decay for a more detailed comparison due to kinematical reasons⁶; it is therefore difficult to explain this discrepancy of the $\pi\pi$ partial width between theory and experiment from our point of view. In ref. [15], we also find an experimental value for the partial width of the decay $f_0(1500) \rightarrow \pi\pi$ which reads $\Gamma_{\text{exp}} = 44.1 \pm 15.3$ MeV. Again, the experimental value is one order of magnitude smaller than the several hundred MeV that we found for the $\pi\pi$ decay modes of the first two states in the f_0 spectrum. Surprisingly, our result for this decay width is 15.7 MeV which is in rough agreement with the experiment due to the destructive interference of the various amplitudes that contribute to this process. Without 't Hooft's six-quark interaction, the pure quark loop result for the partial width would be ≈ 1 MeV which would have clearly underestimated the experimental data. This observation again underlines the importance of the unique feature of our approach, namely the generic inclusion of instanton-induced vertices beyond lowest order for the determination of the strong two-body decay widths. For further results of the 3P_0 model for the f_0 and the f_1 mesons, we refer to the recent preprint of Barnes *et al.* (see [39]).

Let us now turn to a discussion of the other f_0 decay modes which we have not mentioned so far. In tab. 8, we present numerous other results of our calculations with respect to $\eta\eta$, $\sigma\sigma$, KK and other final states. In most cases, we find the correct order of magnitude for the widths although the results are sometimes significantly off the error bars. In fig. 6, we plot the partial widths for the decays $f_0(1500) \rightarrow \pi\pi/\eta\eta/\sigma\sigma/KK$ with respect to the strength of the instanton-induced six quark interaction. The results at $g_{\text{eff}}^{(3)} = 71.4 \text{ GeV}^{-5}$ in general tend to be too large compared with the experimental widths presented in ref. [15]. This fact might hint at a possible re-adjustment of the six-quark coupling constant $g_{\text{eff}}^{(3)}$ at these data; as we have noted before, we have hitherto fixed this constant at the partial width of the decay $K_0^* \rightarrow K\pi$ where it might have been adjusted to a slightly too large numerical value. We shall note at this point that the experimental data in this sector are from one experiment only (see [15]) and that there are no other theoretical calculations such that a detailed comparison might be premature. However, our results seem to be not completely unphysical such that we still consider our approach as a reliable basis for future studies in this field.

Another point to mention here is the flavour structure of the f_J mesons with $J \neq 0$. In general, the ground state is purely $n\bar{n}$ while the next radial excitation is a $s\bar{s}$ state; note that — in contrast to the f_0 mesons — there is no flavour mixing for these mesons as 't Hooft's force only acts on mesons with $J = 0$. This is the reason why the $\pi\pi$ widths of the first excitations of the f_1 , f_2 and f_4 mesons are zero since the quark loop mechanism alone cannot provide a $s\bar{s} \rightarrow n\bar{n} + n\bar{n}$ transition.⁷ The $\pi\pi$ widths of the related ground states are in general too low by orders of magnitudes; as we have already concluded before, the instantaneous Bethe-Salpeter ansatz might not be adequate for the deeply bound pion such that the resulting meson-quark-anti-quark vertex functions are not appropriate for further calculations even in a relativistic framework. The other decay modes of the f_J mesons ($J \neq 0$) are in acceptable agreement with the experimental data; in particular the $f_2(1270)$ and $f'_2(1525)$ decays into KK and $\eta\eta$ final states are excellently described.

⁶As in the decay $\phi(1020) \rightarrow KK$, the exact masses of the outgoing particles in $f_0(1370) \rightarrow \sigma\sigma$ are slightly larger by some MeV than the mass of the decaying particle; in section 4.4, we explain why we refrain from a parameter re-adjustment in such a situation.

⁷For the same reason, we find vanishing decay widths for the decays $f_4(2220) \rightarrow \omega\omega$ and $f_4(2220) \rightarrow a_2\pi$; see tab. 9 for comparison.

4.8 Decays of K_J Mesons

In tab. 10, we summarize our calculations of partial widths for strongly decaying K_J mesons. Let us note that the K_J states for $J \neq 0$ are twice degenerated for each mass due to spins $S = 0$ and $S = 1$ which are not separated by the interquark forces in our model; nevertheless, the number of states in the spectrum is correct (see [11]).

The $K(1460)$ is the first radial excitation of the pseudoscalar kaon in our model. In our calculation, the $K\rho$ mode is quite strong compared to the other final states; this seems to be not unrealistic compared to experiment. Note hereby that the nearly vanishing width for $K(1460) \rightarrow K_0^*(1430)\pi$ is found due to the destructive interference between the approximately equal amplitudes from the quark loop diagram and the instanton-induced six quark vertex contributing to this particular process.

The decays $K_1(1270) \rightarrow K\rho/K^*\pi/K\omega$ are excellently described in our model; here, the 3P_0 model clearly overestimates all widths in this sector. This impressive agreement is exceptional insofar as other kaonic decay modes often suffer from the unrealistic smallness of the calculated partial widths. Indeed, for the next K_1 excitation, our results are less well in agreement with the experiment. Moreover, the $K_2(1580)$ and $K_2(1770)$ decays seem to be clearly underestimated in our approach; the experimental data are however poor and no comparison with the non-relativistic model is possible so far.

4.9 Decays of K_J^* Mesons

As we have already discussing in section 4.1, the value of the strength parameter for 't Hooft's six quark interaction is fixed at the experimental decay width $\Gamma_{\text{exp}} = 274 \pm 37$ MeV of the decay $K_0^*(1430) \rightarrow K\pi$. In fig. 3, we present the related plots not only for the ground state but also for the first radial excitation $K_0^*(1950)$ which is also very well described by our choice $g_{\text{eff}}^{(3)} = 71.4 \text{ GeV}^{-5}$. Thus, the decay widths for $K_0^* \rightarrow K\pi$ presented in tab. 11 are clearly in good agreement with the experimental data since we have adjusted our last free parameter $g_{\text{eff}}^{(3)}$ in this sector. The other decays in this final table involve mesons with $J \neq 0$; they proceed exclusively via quark loop diagrams and are thus not affected by our parameter choice.

It is very interesting to consider the decays $K_J^* \rightarrow K\pi$ with $J = 1, 2, 3, 4, 5$; let us first restrict to ground state K_J^* mesons. For $J = 1$, we find an excellent agreement with the experimental width $\Gamma_{\text{exp}} \approx 50$ MeV. The experimental partial widths for $K\pi$ final states decrease characteristically for increasing total angular momenta J . A comparison with the formula given in eq. (31) shows that this decrease can be approximately traced back to the influence of the phase space factor $\frac{1}{2J_1+1} \cdot \frac{k}{M_1^2}$ such that the matrix element itself should be more or less the same for all $K_J^* \rightarrow K\pi$ decays ($J = 1, \dots, 5$). Unfortunately, this is not correctly described by our model such that our calculation increasingly fails to describe correctly the experimental partial widths for higher angular momenta J . We have already noted that pionic final states might be hard to describe in an instantaneous framework; here, we find another example for this conjecture.

For the other decay modes in this sector, we observe generally a quite poor agreement with experiment as well as with the results of the 3P_0 model. For particular decay channels, our calculation yields more realistic numbers for the partial widths than the non-relativistic model (e.g. for $K_2^*(1430) \rightarrow K\eta$) but, in general, we observe a decreasing accuracy of our results for higher K_J^* excitations and larger total angular momenta. Note however that the calculated large widths for the decays $K_3^*(1780) \rightarrow K^*(892)\rho$ and $K_3^*(1780) \rightarrow K^*(892)\omega$ lead at least to a qualitative understanding of the total decay width in the framework of our model.

4.10 Decays of η_J Mesons

In tab. 13, we present our results concerning the strong decays of the $\eta'(958)$, $\eta(1440)$ and $\eta_2(1645)$ mesons. Their masses are well described in our relativistic quark model; the well-known flavour mixing of the pseudoscalar η mesons is induced by 't Hooft instanton interaction and has been extensively discussed in refs. [11, 34]. We should note that our quark model does not support the hypothesis of the existence of the $\eta(1295)$ meson as a pure $q\bar{q}$ state; it is interesting that in fact no evidence for this state has been found by the CRYSTAL BARREL group (see [16, 19, 35, 36]).

The vanishing decay width of the process $\eta' \rightarrow \rho\pi$ is in agreement with experiment. Some preliminary partial decay widths of the $\eta(1440)$ meson are quoted in ref. [16]; they are given in tab. 13. Our results are in acceptable (and partly excellent) agreement with these experimental data; note that this statement refers to decays that are described by quark loop diagrams only (such as the KK^* final state) as well as to decays in which additional instanton-induced vertices have been considered (such as the $a_0\pi$ and $\sigma\eta$ final states). Concerning the latter decays, the CRYSTAL BARREL group recently found the experimental decay width ratio $R := \Gamma_{\text{exp}}^{a_0\pi}/\Gamma_{\text{exp}}^{\sigma\eta} = 0.62 \pm 0.14$ (see [19]). In our approach, we find $R = 0.43$ which is in reasonable agreement

with this analysis; note that $R = 0.4 \pm 0.2$ has earlier been found in ref. [15] (for more references, see [19]). It is interesting to look at fig. 7 for a more detailed discussion; in this plot, we present the dependence of the decay widths $\eta(1440) \rightarrow a_0\pi$ and $\eta(1440) \rightarrow \sigma\eta$ on the strength of 't Hooft's instanton force. Since the $a_0\pi$ partial width remains more or less constant while the $\sigma\eta$ width is monotonically increasing, a sufficiently large coupling constant $g_{\text{eff}}^{(3)}$ is needed in order to compute a ratio $R < 1$; however, we find again that a slightly smaller value than $g_{\text{eff}}^{(3)} = 71.4 \text{ GeV}^{-5}$ would provide a more exact ratio compared to the experiment quoted in ref. [19]. Finally, the $\eta_2(1645)$ decay widths are smaller than the values obtained in the framework of the 3P_0 model; a more detailed comparison is prevented by the poor accuracy of the experimental data.

5 Summary

In this paper, we have studied strong two-body decays of light mesons. Our approach is based on a relativistic quark model which describes the complete meson spectrum by means of the Bethe-Salpeter equation in its instantaneous approximation. The quark-anti-quark interaction is parameterized by a confinement potential with an appropriate spinorial structure in Dirac space. Furthermore, we adopt 't Hooft's instanton-induced interaction that provides a convincing picture for the well-known mass splittings and flavour mixing effects in the pseudoscalar and scalar meson sector. As we have shown in refs. [11, 12], this formally covariant ansatz leads to an excellent description of the mass spectrum of the light mesons. Furthermore, we have investigated several electroweak decay processes involving light mesons with good results compared to the experimental data; a complete overview on this approach for the intense study of light mesons can be found in ref. [34]. For the calculation of the strong decay widths, we have applied the Mandelstam formalism for the derivation of the related matrix element. Hereby, we have included not only the lowest order quark loop diagrams that contribute to all possible decay modes; moreover, we implemented the three-body interaction of 't Hooft's instanton-induced force that acts on mesons with vanishing total angular momentum. We have thus found that an interference between quark loop diagrams and amplitudes originating in the instanton interaction occurs if all mesons in the decay $\mathcal{M}_1 \rightarrow \mathcal{M}_2\mathcal{M}_3$ have angular momentum $J_i = 0$ ($i = 1, 2, 3$). We shall add that 't Hooft's six quark vertices also provide Zweig rule violating amplitudes contributing to the partial width if and only if at least one of the mesons in the decay process is of isoscalar type. Summarizing, we have calculated the quark loop for each decay and, additionally, the instanton-induced contribution if only mesons with $J_i = 0$ participate in the process under consideration; eventually, OZI forbidden amplitudes might occur due to the latter mechanism if η, η', \dots or f_0, f'_0, \dots mesons are involved in the particular decay.

We have compared our numerical results for the numerous partial decay widths with the experimental data, if possible (see [14] and [15, 16, 17, 18, 19]); in some sectors, these data are quite poor such that more reliable experimental results for the decay width would be extremely helpful to clarify some of the puzzling issues in this field. Moreover, we referred to the so-called 3P_0 model first proposed by A. Le Yaouanc *et al.* (see [1, 2, 3]) which is a non-relativistic approach using quark lines and assuming the creation of an additional quark-anti-quark pair with vacuum quantum numbers $J^{\pi c} = 0^{++}$; the numerical results obtained in this framework were quoted from refs. [6, 7, 8].

Before we summarize our numerical results for the partial widths, we shall note that our approach — similar to the 3P_0 model — does not take into account any final state interaction. The neglect of the related effects is clearly a shortcoming of our ansatz which is, however, hard to overcome in a quark model like the one presented in this publication. We have thus restricted our model to the “impulse approximated” approach although final state interactions are expected to significantly modify the partial widths.

Let us first focus on decays in which only the pure quark loop diagrams contribute to the partial widths. We found that we achieve a description of the strong meson decays that is in parts comparable to the 3P_0 model. However, we also noted that we sometimes underestimate the partial widths by one order of magnitude (or even more) compared to the experiment. This flaw is mostly observed for decays in which one or two pions are in the final state; it might be related to the fact that the underlying instantaneous approximation of the Bethe-Salpeter equation is not suitable for deeply bound states such as the pion ground state. Furthermore, decays of mesons with large angular momentum and decays of highly excited mesons are in general not so well described by the quark loop mechanism alone. It remains an open question whether additional effects due to the final state interaction could modify this observation.

For decays in which instanton-induced vertices beyond the lowest order quark loop diagrams are included, we find that the additional six quark interaction has a strong impact on the numerical results. These decays involve only scalar and pseudoscalar mesons; the related coupling strength $g_{\text{eff}}^{(3)} = 71.4 \text{ GeV}^{-5}$ has been fixed to the decay $K_0^* \rightarrow K\pi$ with $\Gamma_{\text{exp}} = 274 \pm 37 \text{ MeV}$. In this example, 't Hooft's three-body force lifts the partial decay width from a few MeV from the pure quark loop mechanism up to several hundred

MeV in excellent agreement with the experiment. Here, the interference between both mechanisms was constructive; we have however discussed several other decay modes in which the interference was destructive. The interference between quark loop amplitudes and instanton-induced amplitudes can be translated into an interference between OZI allowed and OZI forbidden amplitudes if isoscalar mesons are involved. In these cases, we discussed numerous examples in which the (constructive or destructive) interference between both contributions led to very realistic results for the partial decay widths. In general, we found that the additional instanton-induced mechanism significantly modified the result of the pure quark loop calculation. Hereby, we discussed that the conventional conclusion concerning the flavour contents of resonances, which may be roughly formulated as “dominant $\pi\pi$ decay mode indicates large nonstrange contents in the decaying resonance” and “dominant $K\bar{K}$ decay mode indicates large strange contents in the decaying resonance”, is not true for mesons that can decay via the Zweig rule violating part of the instanton induced six-quark interaction and may be misleading. Summarizing, we presented impressing examples for the importance of this contributions beyond lowest order and concluded that, apart from the quark loop diagrams, the inclusion of additional effects at least for scalar and pseudoscalar meson decays seems to be mandatory.

For future studies, it might be helpful to consider effects that are not included in our approach such as final state interactions or other mechanisms beyond lowest order or instanton-induced vertices; moreover, more experimental data are clearly needed for a better assessment of the various theoretical models for this problem. The study of strong mesons decays thus remains a challenge for theory and experiment as well. However, we believe that the present publication provides a reliable framework for a detailed investigation of strong meson decays as it is based on a completely covariant approach and includes realistic mechanisms for the description of the decay processes.

Acknowledgements

We have profited very much from discussions with H.-R. Petry, J.-S. Suh, B. Pick, J. Reinnarth, A. V. Sarantsev and E. Shuryak to whom we wish to express our gratitude. Furthermore, we thank V. Hellmann for useful numerical checks and careful reading of the manuscript. Financial support of the DEUTSCHE FORSCHUNGSGEMEINSCHAFT is gratefully acknowledged.

References

- [1] A. Le Yaouanc, L. Oliver, O. Pene and J. C. Raynal, Phys. Rev. D **8** (1973) 2223.
- [2] A. Le Yaouanc, L. Oliver, O. Pene and J. C. Raynal, Phys. Rev. D **9** (1974) 1415.
- [3] A. Le Yaouanc, L. Oliver, O. Pene and J. C. Raynal, Phys. Rev. D **11** (1975) 1272.
- [4] A. Le Yaouanc, L. Oliver, O. Pene and J. C. Raynal, “Hadron Transitions In The Quark Model”. New York, USA: Gordon & Breach (1988), 311 p.
- [5] L. Micu, Nucl. Phys. B **10** (1969) 521.
- [6] E. S. Ackleh, T. Barnes and E. S. Swanson, Phys. Rev. D **54** (1996) 6811.
- [7] T. Barnes, F. E. Close, P. R. Page, E. S. Swanson, Phys. Rev. D **55** 4157 (1997).
- [8] R. Bonnaz and B. Silvestre-Brac, Few Body Syst. **30** (2001) 223.
- [9] J. Resag, C. R. Münz, B. C. Metsch, H. R. Petry, Nucl. Phys. **A578** (1994) 397.
- [10] J. Resag, C. R. Münz, B. C. Metsch, H. R. Petry, Nucl. Phys. **A578** (1994) 418.
- [11] M. Koll, R. Ricken, D. Merten, B. C. Metsch and H. R. Petry, Eur. Phys. J. A **9** (2000) 73.
- [12] R. Ricken, M. Koll, D. Merten, B. C. Metsch and H. R. Petry, Eur. Phys. J. A **9** (2000) 221.
- [13] C. Ritter, B. C. Metsch, C. R. Münz, H. R. Petry, Phys. Lett. **B380** (1996) 431.
- [14] PARTICLE DATA GROUP, D. E. Groom *et al.*, Eur. Phys. J. **C15** (2000) 1.
- [15] A. Abele *et al.* [CRYSTAL BARREL Collaboration], Eur. Phys. J. C **21** (2001) 261.
- [16] J.-S. Suh, *Untersuchung des E-Mesons in der Proton-Antiproton-Vernichtung in Ruhe*, Doctoral Thesis, University of Bonn, 1999.
- [17] D. Barberis *et al.* [WA102 Collaboration], Phys. Lett. B **471** (2000) 440.
- [18] D. V. Bugg, B. S. Zou and A. V. Sarantsev, Nucl. Phys. B **471** (1996) 59.
- [19] J. Reinnarth *et al.* [CB@LEAR Collaboration], *The investigation of the E-meson in the reaction $\bar{p}p \rightarrow \pi^+\pi^-\pi^+\pi^-\eta$* , manuscript (in preparation), University of Bonn, 2002.
- [20] G. 't Hooft, Phys. Rev. D **14** (1976) 3432 [Erratum: *ibid.* D **18** (1976) 2199].
- [21] M. A. Shifman, A. I. Vainshtein and V. I. Zakharov, Nucl. Phys. B **163** (1980) 46.
- [22] H. R. Petry, H. Hofestadt, S. Merk, K. Bleuler, H. Bohr and K. S. Narain, Phys. Lett. B **159** (1985) 363.
- [23] E. E. Salpeter, H. A. Bethe, Phys. Rev. **84** (1951) 1232.
- [24] E. E. Salpeter, Phys. Rev. **87** (1952) 328.
- [25] S. Mandelstam, Proc. Roy. Soc. **233**, **248** (1955).
- [26] W. H. Blask, U. Bohn, M. G. Huber, B. C. Metsch and H. R. Petry, Z. Phys. A **337** (1990) 327.
- [27] B. Ch. Metsch, *Instanton-Induzierte Quarkkräfte und Hadronspektroskopie*, Habilitation Thesis, University of Bonn, 1993.
- [28] U. Löring, K. Kretzschmar, B. C. Metsch and H. R. Petry, Eur. Phys. J. A **10** (2001) 309.
- [29] U. Loring, B. C. Metsch and H. R. Petry, Eur. Phys. J. A **10** (2001) 395.
- [30] U. Löring, B. C. Metsch and H. R. Petry, Eur. Phys. J. A **10** (2001) 447.
- [31] C. Ritter, *Instantoninduzierte Zerfälle skalarer und pseudoskalarer Mesonen*, Diploma Thesis, ITKP, University of Bonn, Germany (1996).
- [32] R. Ricken, *Properties of Light Mesons in a Relativistic Quark Model*, Doctoral Thesis, ITKP, University of Bonn, Germany (2001).
- [33] V. V. Anisovich, *The lightest scalar glueball: Retrospective view and the current state of the problem*. Prepared for 7th International Conference on Hadron Spectroscopy (Hadron 97), Upton, NY, 25-30 Aug 1997; Phys. Usp. **41** (1998) 419 [Usp. Fiz. Nauk **168** (1998) 481]; see also hep-ph/9712504.
- [34] M. Koll, *Electroweak Processes with Light Mesons in a Relativistic Quark Model*, Doctoral Thesis, ITKP, University of Bonn, Germany (2001) [see also <http://www.itkp.uni-bonn.de/~koll>].
- [35] J. S. Suh [Crystal Barrel Collaboration], Nucl. Phys. A **675** (2000) 100C.
- [36] J. S. Suh [Crystal Barrel Collaboration], Nucl. Phys. A **675** (2000) 104C.
- [37] A. Abele *et al.* [Crystal Barrel Collaboration], Eur. Phys. J. C **19** (2001) 667.
- [38] D. Jarecke, P. Maris and P. C. Tandy, [nucl-th/0208019](http://arxiv.org/abs/nucl-th/0208019).
- [39] T. Barnes, N. Black and P. R. Page, [nucl-th/0208072](http://arxiv.org/abs/nucl-th/0208072).

A Flavour Factors and Charge Multiplicities

For the calculation of the general (*i.e.* charge independent) widths of decays like $\rho \rightarrow \pi\pi$ instead of a special process with definite charges like $\rho^+ \rightarrow \pi^+\pi^0$, it is well known that one only needs to sum over all possible final states and to average over all possible initial states. Using isospin symmetry, this operation links the special decay width $\Gamma_{\mathcal{M}_1 \rightarrow \mathcal{M}_2 \mathcal{M}_3}^{\text{special}}$ with the general decay width $\Gamma_{\mathcal{M}_1 \rightarrow \mathcal{M}_2 \mathcal{M}_3}^{\text{general}}$ by the use of a Clebsch–Gordan coefficient $C := \langle I_2 m_2 | I_3 m_3 | I_1 m_1 \rangle$; here, I_k denotes the isospin with its third component m_k ($k = 1, 2, 3$). For bosonic particles in the final states such as mesons, one has to add a symmetry factor $\frac{1}{2}$ if both outgoing particles are identical; note that this factor of course must not be multiplied for a $K\bar{K}$ final state. Thus, the expression

$$\Gamma_{\mathcal{M}_1 \rightarrow \mathcal{M}_2 \mathcal{M}_3}^{\text{general}} = \Gamma_{\mathcal{M}_1 \rightarrow \mathcal{M}_2 \mathcal{M}_3}^{\text{special}} \frac{1 - \frac{1}{2}\delta_{\mathcal{M}_2 \mathcal{M}_3}}{\left| \langle I_2 m_2 | I_3 m_3 | I_1 m_1 \rangle \right|^2} \quad (34)$$

yields the correct general decay width $\Gamma_{\mathcal{M}_1 \rightarrow \mathcal{M}_2 \mathcal{M}_3}^{\text{general}}$ although in fact only the particular width $\Gamma_{\mathcal{M}_1 \rightarrow \mathcal{M}_2 \mathcal{M}_3}^{\text{special}}$ is numerically computed (see also [6]). Note that the evaluation of the flavour trace in the decay matrix element actually yields a factor f which clearly depends on the particular charge distribution in the special decay. As examples, we quote $f^2(K^{*+} \rightarrow K^0\pi^+) = 1$ and $f^2(K^{*+} \rightarrow K^+\pi^0) = \frac{1}{2}$ for the decay of an isodoublet meson into an isodoublet meson and an isovector meson. Here, the Clebsch–Gordan coefficients $C^2(K^{*+} \rightarrow K^0\pi^+) = \frac{1}{3}$ and $C^2(K^{*+} \rightarrow K^+\pi^0) = \frac{2}{3}$ in isospin space are different for both decay types such that the fraction $\mathcal{F}_{K^* \rightarrow K\pi} := f_{K^* \rightarrow K\pi}^2 / C_{K^* \rightarrow K\pi}^2 = 3$ is constant. For the sake of clarity, we quote all possible flavour weight factors in tab. 2; we refer to ref. [6] for further comments.

B The Instanton–Induced 't Hooft Interaction

Following G. 't Hooft's seminal ideas on instantons in QCD first published in ref. [20], M. A. Shifman, A. I. Vainshtein and V. I. Zakharov have derived the Lagrangian $\Delta\mathcal{L}^{\text{eff}}$ describing the contribution of instanton–anti-instanton configurations to the effective Lagrangian for light quarks (see [21]). Their result is discussed in ref. [10] with respect to the relativistic quark model for mesons which provides the basis for the present contribution.

Omitting the confining interaction for a moment, we can write down the following effective Lagrangian mimicking the QCD dynamics in our model:

$$\mathcal{L}_{\text{QCD}}^{\text{eff}} = \mathcal{L}_{\text{QCD}}^0 + \Delta\mathcal{L}^{\text{eff}} = k + \sum_{f=1}^3 : \bar{\Psi}_f (i\partial - m_f) \Psi_f : + \mathcal{L}^{(2)} + \mathcal{L}^{(3)} \quad ; \quad (35)$$

here, $\mathcal{L}_{\text{QCD}}^0 = \sum_{f=1}^3 \bar{\Psi}_f (i\partial - m_f^0) \Psi_f$ is the free quark Lagrangian with current quark masses m_f^0 (for the flavour index, $f = \{1, 2, 3\} = \{u, d, s\}$ holds). In $\mathcal{L}_{\text{QCD}}^{\text{eff}}$, the masses $m_f = m_f^0 + \Delta m_f$ are constituent quark masses with a characteristic contribution Δm_f to the effective mass due to instanton effects (see [10]). The constant k denotes the vacuum energy density and is inessential for our present considerations. The contributions $\mathcal{L}^{(2)}$ and $\mathcal{L}^{(3)}$ represent the two–body and the three–body interactions, respectively; we will briefly discuss these terms in the following

B.1 The Two–Body Interaction

As it has been discussed in ref. [10], the relativistic quark model used in this publication incorporates a particular residual interaction besides the global confining interaction. It is described by the two–body term in 't Hooft's instanton–induced force and reads explicitly

$$\mathcal{L}^{(2)} = g_{\text{eff}}^{(2)}(i) \frac{3}{16} \left[: \bar{\Psi}_k \bar{\Psi}_l (\mathbb{1} \otimes \mathbb{1} + \gamma_5 \otimes \gamma_5) \epsilon_{ikl} \epsilon_{imn} (2\mathcal{P}_3^C + \mathcal{P}_6^C) \Psi_m \Psi_n : \right]. \quad (36)$$

Here, a summation over the flavour indices $i, k, l, m, n = \{1, 2, 3\} = \{u, d, s\}$ is understood. Note that \mathcal{P}_3^C denotes the projector onto colour anti–triplet and \mathcal{P}_6^C denotes the projector onto colour sextet.

This instanton-induced two-body interaction only acts on $q\bar{q}$ bound states with total angular momentum $J = 0$, *i.e.* for pseudoscalar and scalar mesons. Its effects on the mass spectrum of these states are highly interesting; they have been intensively discussed in refs. [11, 12]. In our calculations for light mesons, we assume SU(2) flavour invariance and define for practical reasons the coupling constants $g := \frac{3}{8}g_{\text{eff}}^{(2)}(s)$ and $g' := \frac{3}{8}g_{\text{eff}}^{(2)}(n)$ where s and n denotes “strange” and “non-strange” quarks, respectively. Note that this interaction also provides a realistic mechanism for the well-known flavour mixing effect in the isoscalar states. In this appendix, we refrain from a discussion of this particular aspect and also of further implications of the use of this residual interaction in our quark model; instead, we refer to former publications for more details (see [11, 12] and references therein).

B.2 The Three-Body Interaction

The three-body term $\mathcal{L}^{(3)}$ in eq. (35) does not influence the spectroscopical results for $q\bar{q}$ mesons; interestingly, it does neither contribute to baryons described by colourless qqq bound states (see [29]). However, it has been shown in refs. [13, 31, 32] that the three-body term of 't Hooft's interaction generates additional contributions to strong two-body decays beyond the pure quark loop part if all mesons participating the process have vanishing angular momenta, *i.e.* $J_1 = J_2 = J_3 = 0$. Written out explicitly, the term reads

$$\mathcal{L}^{(3)} = g_{\text{eff}}^{(3)} \frac{27}{80} \left[: \bar{\Psi} \bar{\Psi} \bar{\Psi} (\mathbb{I} \otimes \mathbb{I} \otimes \mathbb{I} + (\gamma_5 \otimes \gamma_5 \otimes \mathbb{I} + \text{cycl. perm.})) \mathcal{P}_1^F (2\mathcal{P}_{10}^C + 5\mathcal{P}_8^C) \Psi \Psi \Psi : \right] \quad (37)$$

where \mathcal{P}_1^F is a projector onto a three-particle flavour singlet state and \mathcal{P}_{10}^C (\mathcal{P}_8^C) is a projector onto colour decuplet (octet). Due to the special Dirac structure of this interaction, it can be written more convenient by using the Weyl representation of the Dirac spinors, *i.e.*

$$\Psi(x) = \begin{pmatrix} \xi(x) \\ \eta(x) \end{pmatrix} \quad (38)$$

and γ_5 is diagonal in this representation. Then we can express the three-body term of 't Hooft's instanton-induced interaction according to

$$\mathcal{L}^{(3)} = g_{\text{eff}}^{(3)} \frac{27}{30} \left[: \eta^\dagger \eta^\dagger \eta^\dagger \mathcal{O}^{FSC} \xi \xi \xi : \right] + (\eta \longleftrightarrow \xi) . \quad (39)$$

Here, the operator \mathcal{O}^{FSC} acts in flavour, spin and colour space and reads explicitly

$$\mathcal{O}^{FSC} := 2\mathcal{P}_1^F \otimes \mathcal{P}_4^S \otimes \mathcal{P}_{10}^C + 5\mathcal{P}_1^F \otimes \mathcal{P}_2^S \otimes \mathcal{P}_8^C \quad (40)$$

where \mathcal{P}_2^S (\mathcal{P}_4^S) is a projector onto spin doublet (quadruplet). Note that the overall flavour projector \mathcal{P}_1^F in the operator \mathcal{O}^{FSC} leads to a violation of the phenomenological OZI rule if one of the particles in the decay process is an isoscalar meson; this point is briefly discussed in section 3.5.

C Tables and Figures

C.1 Tables

	Parameter		This work
't Hooft interaction	g g' $g_{\text{eff}}^{(3)}$ Λ_{III}	$[\text{GeV}^{-2}]$ $[\text{GeV}^{-2}]$ $[\text{GeV}^{-5}]$ $[\text{fm}]$	1.62 1.35 71.4 0.42
Constituent quark masses	m_n m_s	$[\text{MeV}]$ $[\text{MeV}]$	380 550
Confinement parameters	a_c b_c	$[\text{MeV}]$ $[\text{MeV}/\text{fm}]$	-1135 1300
Spin structure	$\Gamma \otimes \Gamma$		$\frac{1}{2}(\mathbb{1} \otimes \mathbb{1} - \gamma_\mu \otimes \gamma^\mu - \gamma^5 \otimes \gamma^5)$

Table 1: The parameters of the confinement force, the 't Hooft interaction and the constituent quark masses in this work; the particular values of this parameter set correspond to model \mathcal{B} first presented and discussed in refs. [11, 12]. Note that the three-body 't Hooft coupling $g_{\text{eff}}^{(3)}$ appears in this work for the first time; it has been adjusted to the experimental width of the decay $K_0^* \rightarrow K\pi$.

I_1	I_2	I_3	Example	$\mathcal{F}_{\mathcal{M}_1 \rightarrow \mathcal{M}_2 \mathcal{M}_3}$
0	0	0	$f_2 \rightarrow \eta\eta^\dagger$	1
$\frac{1}{2}$	0	$\frac{1}{2}$	$K^* \rightarrow K\eta'$	1
1	0	1	$a_2 \rightarrow \pi\eta$	1
0	$\frac{1}{2}$	$\frac{1}{2}$	$f_0 \rightarrow K\bar{K}$	2
1	$\frac{1}{2}$	$\frac{1}{2}$	$a_0 \rightarrow K\bar{K}$	1
$\frac{1}{2}$	$\frac{1}{2}$	1	$K_2^* \rightarrow K\pi$	3
0	1	1	$f_0 \rightarrow \pi\pi^\dagger$	$3/2$
1	1	1	$\rho \rightarrow \pi\pi^\dagger$	1

Table 2: Flavour weight factors for the various isospin channels of the strong two-body decay $\mathcal{M}_1 \rightarrow \mathcal{M}_2 \mathcal{M}_3$; see text for details. Note that for the examples marked with \dagger an additional factor of $\frac{1}{2}$ for identical mesons in the final state is included.

Final State	Experimental Partial Width	3P_0 Model (Refs. [6, 7])	This Work	incl. III	incl. ZRV
$\rho(770)$, $\Gamma_{\text{exp}}^{\text{total}} = 150.2 \pm 0.8$ MeV					
$\pi\pi$	≈ 150	79	42.9	○	○
$\rho(1450)$, $\Gamma_{\text{exp}}^{\text{total}} = 310 \pm 60$ MeV					
$\pi\pi$	seen	74	2.37	○	○
$\omega\pi$	< 6.2	122	0.00	○	○
$\rho\eta$	< 12.4	25	0.09	○	○
KK	< 0.50	35	0.03	○	○
$\rho(1700)$, $\Gamma_{\text{exp}}^{\text{total}} = 240 \pm 60$ MeV					
$\pi\pi$	seen	48	1.16	○	○
$\omega\pi$	seen	35	1.58	○	○
$\rho\eta$	< 9.6	16	2.82	○	○
KK	seen	36	1.99	○	○
$\rho_3(1690)$, $\Gamma_{\text{exp}}^{\text{total}} = 161 \pm 10$ MeV					
$\pi\pi$	38 ± 3.2	59	0.82	○	○
$\omega\pi$	18.3 ± 7.0	19	2.92	○	○
$\rho\eta$	seen	2	4.10	○	○
KK	2.54 ± 0.45	9	6.37	○	○
$\rho\rho$	—	71	55.6	○	○

Table 3: Results on strong two-body decays of (excited) isovector ρ_J mesons. All widths are given in units of [MeV]; the experimental data are extracted from ref. [14]. The column “III” denotes whether effects of the instanton-induced three-body interaction are included (●) or not (○). In the column “ZRV”, we indicate whether Zweig rule violation due to the presence of isoscalar mesons in the instanton-induced mechanism occurs (●) or not (○).

Final State	Experimental Partial Width	3P_0 Model (Ref. [7])	This Work	incl. III	incl. ZRV
$\pi(1300)$, $\Gamma_{\text{exp}}^{\text{total}} = 200 \dots 600$ MeV					
$\rho\pi$	seen	209	2.57	○	○
$\pi(1800)$, $\Gamma_{\text{exp}}^{\text{total}} = 210 \pm 15$ MeV					
$\rho\pi$	not seen	31	0.34	○	○
$\rho\omega$	—	73	1.46	○	○
$f_0(1370)\pi$	seen	7	1.12	●	●
$f_0(1500)\pi$	seen	—	3.05	●	●
$f_2(1270)\pi$	—	28	4.16	○	○
$a_0(980)\eta$	seen	—	2.79	●	●
KK_0^*	seen	—	0.02	●	○
KK^*	not seen	36	1.76	○	○
$\pi_2(1670)$, $\Gamma_{\text{exp}}^{\text{total}} = 259 \pm 11$ MeV					
$\rho\pi$	84 ± 11	118	12.3	○	○
$\rho\omega$	7.0 ± 2.9	41	0.11	○	○
$\sigma\pi$	34 ± 16	—	14.7	○	○
$f_0(1370)\pi$	24 ± 9	0	0.26	○	○
$f_2(1270)\pi$	152 ± 11	75	6.16	○	○
KK^*	11 ± 4	30	5.18	○	○

Table 4: Results on strong two-body decays of (excited) isovector π_J mesons. All widths are given in units of [MeV]; the experimental data are extracted from ref. [14]. For further comments, see text and caption of tab. 3.

Final State	Experimental Partial Width	3P_0 Model (Refs. [7, 8])	This Work	incl. III	incl. ZRV
$\omega(782)$, $\Gamma_{\text{exp}}^{\text{total}} = 8.44 \pm 0.09$ MeV					
$\pi\pi$	0.19 ± 0.03	—	0.00	○	○
$\omega(1420)$, $\Gamma_{\text{exp}}^{\text{total}} = 174 \pm 59$ MeV					
$\rho\pi$	dominant	328	4.73	○	○
$\eta\omega$	—	12	2.82	○	○
$b_1(1235)\pi$	—	1	0.17	○	○
KK	—	31	1.99	○	○
$\omega_3(1670)$, $\Gamma_{\text{exp}}^{\text{total}} = 168 \pm 10$ MeV					
$\rho\pi$	seen	50	8.76	○	○
$\eta\omega$	—	2	4.10	○	○
$b_1(1235)\pi$	possibly seen	7	3.33	○	○
KK	—	8	6.37	○	○
$\phi(1020)$, $\Gamma_{\text{exp}}^{\text{total}} = 4.46 \pm 0.03$ MeV					
KK	2.19 ± 0.04	4.08	—	○	○
$\pi\pi$	$(0.33 \pm 0.06) \cdot 10^{-3}$	—	0.00	○	○
$\omega\pi$	$(0.21 \pm 0.09) \cdot 10^{-3}$	—	0.00	○	○
$\phi(1680)$, $\Gamma_{\text{exp}}^{\text{total}} = 150 \pm 50$ MeV					
KK	dominant	—	7.83	○	○
KK^*	seen	—	4.11	○	○
$\phi_3(1850)$, $\Gamma_{\text{exp}}^{\text{total}} = 87^{+28}_{-23}$ MeV					
KK	seen	—	26.7	○	○
KK^*	seen	—	13.8	○	○

Table 5: Results on strong two-body decays of (excited) isoscalar ω_J and ϕ_J mesons. All widths are given in units of [MeV]; the experimental data are extracted from ref. [14]. Note that the $\omega(1420)$ is considered to be a dominantly S -wave state in ref. [7]; therefore we identify it with the second $n\bar{n}$ excitation in the ω/ϕ system (see [11, 34]). For the same reason, we assume that the $\phi(1680)$ is the second $s\bar{s}$ excitation in the ω/ϕ system. For further comments, see text and caption of tab. 3.

Final State	Experimental Partial Width	3P_0 Model (Refs. [6, 7])	This Work	incl. III	incl. ZRV
$h_1(1170)$, $\Gamma_{\text{exp}}^{\text{total}} = 360 \pm 40$ MeV					
$\rho\pi$	seen	383	50.6	○	○
$h_1(1700)$, $\Gamma_{\text{exp}}^{\text{total}}$ unknown					
$\rho\pi$	—	173	5.16	○	○
$\omega\eta$	—	17	0.99	○	○
$\rho(1465)\pi$	—	31	15.3	○	○
$b_1(1235)\pi$	—	0	0.00	○	○
KK^*	—	30	0.52	○	○
$h_3(2050)$, $\Gamma_{\text{exp}}^{\text{total}}$ unknown					
$\rho\pi$	—	115	6.38	○	○
$\omega\eta$	—	13	5.91	○	○
$\rho(1465)\pi$	—	1	13.1	○	○
$b_1(1235)\pi$	—	0	0.00	○	○
KK^*	—	22	2.73	○	○
$b_1(1235)$, $\Gamma_{\text{exp}}^{\text{total}} = 142 \pm 9$ MeV					
$\omega\pi$	seen	143	16.9	○	○
$b_1(1700)$, $\Gamma_{\text{exp}}^{\text{total}}$ unknown					
$\omega\pi$	—	—	1.72	○	○
$\rho\eta$	—	18	0.99	○	○
$\rho\rho$	—	60	0.70	○	○
$a_2(1320)\pi$	—	67	6.51	○	○
KK^*	—	30	0.52	○	○
$b_3(2050)$, $\Gamma_{\text{exp}}^{\text{total}}$ unknown					
$\omega\pi$	—	37	2.13	○	○
$\rho\eta$	—	13	5.91	○	○
$\rho\rho$	—	33	0.02	○	○
$a_2(1320)\pi$	—	107	3.59	○	○
KK^*	—	22	2.73	○	○

Table 6: Results on strong two-body decays of (excited) isoscalar h_J and isovector b_J mesons. All widths are given in units of [MeV]; the experimental data are extracted from ref. [14]. The $n\bar{n}$ states $h_1(1700)$, $h_3(2050)$, $b_1(1700)$ and $b_3(2050)$ are not listed in ref. [14] by the PARTICLE DATA GROUP; however, the assumptions of the 3P_0 model concerning their masses fit very well to the results of our quark model (see [11, 34]). For further comments, see text and caption of tab. 3.

Final State	Experimental Partial Width	3P_0 Model (Refs. [6, 7, 8])	This Work	incl. III	incl. ZRV
$a_0(980)$, $\Gamma_{\text{exp}}^{\text{total}} = 50 \dots 100$ MeV					
$\eta\pi$	dominant	—	70.2	•	•
KK	seen	—	42.9	•	○
$a_0(1450)$, $\Gamma_{\text{exp}}^{\text{total}} = 265 \pm 13$ MeV					
$\eta\pi$	seen	5	31.4	•	•
$\eta'\pi$	seen	5	12.7	•	•
KK	seen	0	64.7	•	○
$a_1(1260)$, $\Gamma_{\text{exp}}^{\text{total}} = 250 \dots 600$ MeV					
$\rho\pi$	seen	545	11.9	○	○
$\sigma\pi$	seen	—	7.18	○	○
$a_1(1640)$, $\Gamma_{\text{exp}}^{\text{total}} = 300 \pm 50$ MeV					
$f_2(1270)\pi$	seen	39	0.32	○	○
$\sigma\pi$	seen	—	0.58	○	○
$a_2(1320)$, $\Gamma_{\text{exp}}^{\text{total}} = 104.7 \pm 1.9$ MeV					
$\rho\pi$	77.3 ± 5.4	34.3	15.0	○	○
$\eta\pi$	16.0 ± 1.3	8.01	8.67	○	○
$\eta'\pi$	0.59 ± 0.10	0.56	1.07	○	○
KK	5.40 ± 0.88	5.24	11.7	○	○
$a_4(2040)$, $\Gamma_{\text{exp}}^{\text{total}} = 361 \pm 50$ MeV					
$\rho\pi$	seen	33	2.17	○	○
$\rho_3\pi$	—	2	0.85	○	○
$f_2(1270)\pi$	seen	10	0.69	○	○

Table 7: Results on strong two-body decays of (excited) isovector a_J mesons. All widths are given in units of [MeV]; the experimental data are extracted from ref. [14]. In the 3P_0 model, the second radial excitation of the a_0 meson is assumed to have a mass around $M_{a'_0} \approx 1700$ MeV (see [7]). Note that the different versions of the 3P_0 model give partly different results for the decay widths, *e.g.* $\Gamma(a_2 \rightarrow \rho\pi) = 54$ MeV in ref. [7] but $\Gamma(a_2 \rightarrow \rho\pi) = 34$ MeV in ref. [8]; in the table, we use the results of ref. [8] concerning the partial widths of the $a_2(1320)$ meson for comparison. For further comments, see text and caption of tab. 3.

Final State	Experimental Partial Width	3P_0 Model (Ref. [6])	This Work	incl. III	incl. ZRV
$f_0(400 \dots 1200)$, $\Gamma_{\text{exp}}^{\text{total}} = 600 \dots 1000$ MeV					
$\pi\pi$	dominant	—	297	●	●
$f_0(1370)$, $\Gamma_{\text{exp}}^{\text{total}} = 275 \pm 55$ MeV					
$\pi\pi$	21.7 ± 9.9	271	477	●	●
$\eta\eta$	0.41 ± 0.27	—	6.25	●	●
$\sigma\sigma$	120.5 ± 45.2	—	—	●	●
$\rho\rho$	62.2 ± 28.8	—	—	○	○
KK	$5.2 \dots 28.4$	—	34.7	●	●
$a_1(1260)\pi$	14.1 ± 7.2	—	—	○	○
$f_0(1500)$, $\Gamma_{\text{exp}}^{\text{total}} = 130 \pm 30$ MeV					
$\pi\pi$	44.1 ± 15.3	—	15.7	●	●
$\pi(1300)\pi$	35.5 ± 29.2	—	1.40	●	●
$\eta\eta$	3.4 ± 1.2	—	20.2	●	●
$\eta\eta'$	2.9 ± 1.0	—	0.08	●	●
$\sigma\sigma$	18.6 ± 12.5	—	37.9	●	●
$\rho\rho$	8.9 ± 8.2	—	—	○	○
KK	8.1 ± 2.8	—	27.7	●	●
$a_1(1260)\pi$	8.6 ± 6.6	—	2.11	○	○
$f_1(1285)$, $\Gamma_{\text{exp}}^{\text{total}} = 24.0 \pm 1.2$ MeV					
$a_0(980)\pi$	8.64 ± 1.73	—	0.06	○	○
$f_1(1420)$, $\Gamma_{\text{exp}}^{\text{total}} = 55.0 \pm 2.9$ MeV					
$a_0(980)\pi$	—	—	0.00	○	○
KK^*	dominant	—	3.41	○	○

Table 8: Results on strong two-body decays of (excited) isoscalar f_J mesons with $J = 0, 1$. All widths are given in units of [MeV]. The experimental data for the $f_0(1370)$ and $f_0(1500)$ decays are extracted from ref. [15]; the rest is given in ref. [14]. Note that the $f_0(400 \dots 1200)$ meson is usually labeled “ σ ” in this work. For further comments, see text and caption of tab. 3.

Final State	Experimental Partial Width	3P_0 Model (Ref. [8])	This Work	incl. III	incl. ZRV
$f_2(1270)$, $\Gamma_{\text{exp}}^{\text{total}} = 185.1^{+3.4}_{-2.6}$ MeV					
$\pi\pi$	$156.9^{+3.8}_{-1.3}$	144	6.33	○	○
KK	8.6 ± 0.8	8.53	11.7	○	○
$\eta\eta$	0.83 ± 0.18	1.02	3.48	○	○
$f'_2(1525)$, $\Gamma_{\text{exp}}^{\text{total}} = 76 \pm 10$ MeV					
$\pi\pi$	0.60 ± 0.12	—	0.00	○	○
KK	65^{+5}_{-4}	82.8	60.5	○	○
$\eta\eta$	7.6 ± 2.5	7.84	7.86	○	○
$f_4(2050)$, $\Gamma_{\text{exp}}^{\text{total}} = 222 \pm 19$ MeV					
$\pi\pi$	seen	—	0.29	○	○
KK	seen	—	1.86	○	○
$f_4(2220)$, $\Gamma_{\text{exp}}^{\text{total}} = 23^{+8}_{-7}$ MeV					
$\pi\pi$	37.7 ± 4.6	53.1	0.00	○	○
KK	$1.51^{+0.77}_{-0.42}$	0.25	8.74	○	○
$\eta\eta$	0.47 ± 0.18	4.62	1.17	○	○
$\omega\omega$	57.7 ± 14.2	23.6	0.00	○	○
$a_2(1320)\pi$	seen	—	0.00	○	○
$f_6(2510)$, $\Gamma_{\text{exp}}^{\text{total}} = 255 \pm 40$ MeV					
$\pi\pi$	15.3 ± 3.5	—	0.02	○	○
KK	—	—	0.11	○	○

Table 9: Results on strong two-body decays of (excited) isoscalar f_J mesons with $J = 2, 4, 6$. All widths are given in units of [MeV]; the experimental data are extracted from ref. [14]. According to the PARTICLE DATA GROUP, the total angular momentum of the $f_J(2220)$ could either be $J = 2$ or $J = 4$ (see [14]); here, we consider this meson as the first $s\bar{s}$ excitation of the f_4 system with $I(J^{\pi^c}) = 0(4^{++})$. For further comments, see text and caption of tab. 3.

Final State	Experimental Partial Width	3P_0 Model (Ref. [8])	This Work	incl. III	incl. ZRV
$K(1460)$, $\Gamma_{\text{exp}}^{\text{total}} \approx 250 \dots 260$ MeV					
$K\rho$	seen	—	56.7	○	○
$K^*(892)\pi$	seen	—	0.11	○	○
$K_0^*(1430)\pi$	seen	—	0.01	●	○
$K_1(1270)$, $\Gamma_{\text{exp}}^{\text{total}} = 90 \pm 20$ MeV					
$K\rho$	37.8 ± 10.0	118	29.0	○	○
$K^*(892)\pi$	14.4 ± 5.5	29.6	14.1	○	○
$K\omega$	9.9 ± 2.8	23.0	7.69	○	○
$K_1(1400)$, $\Gamma_{\text{exp}}^{\text{total}} = 174 \pm 13$ MeV					
$K\rho$	2 ± 1	77.8	22.0	○	○
$K^*(892)\pi$	117 ± 10	319	13.9	○	○
$K\omega$	23 ± 12	31.6	7.40	○	○
$K_2(1580)$, $\Gamma_{\text{exp}}^{\text{total}} \approx 110$ MeV					
$K^*(892)\pi$	seen	—	0.69	○	○
$K_2^*(1430)\pi$	possibly seen	—	0.74	○	○
$K\phi$	—	—	0.78	○	○
$K\omega$	—	—	5.48	○	○
$K_2(1770)$, $\Gamma_{\text{exp}}^{\text{total}} = 186 \pm 14$ MeV					
$K^*(892)\pi$	seen	—	6.84	○	○
$K_2^*(1430)\pi$	dominant	—	2.28	○	○
$K\phi$	seen	—	4.37	○	○
$K\omega$	seen	—	4.91	○	○

Table 10: Results on strong two-body decays of (excited) isodoublet K_J mesons. All widths are given in units of [MeV]; the experimental data are extracted from ref. [14]. For further comments, see text and caption of tab. 3.

Final State	Experimental Partial Width	3P_0 Model (Ref. [8])	This Work	incl. III	incl. ZRV
$K_0^*(1430)$, $\Gamma_{\text{exp}}^{\text{total}} = 294 \pm 23$ MeV					
$K\pi$	274 ± 37	455.8	274	•	○
$K_0^*(1950)$, $\Gamma_{\text{exp}}^{\text{total}} = 201 \pm 86$ MeV					
$K\pi$	105 ± 52	—	80.5	•	○
$K^*(892)$, $\Gamma_{\text{exp}}^{\text{total}} = 50.8 \pm 0.9$ MeV					
$K\pi$	≈ 50	33.9	48.3	○	○
$K^*(1410)$, $\Gamma_{\text{exp}}^{\text{total}} = 232 \pm 21$ MeV					
$K^*(892)\pi$	> 93	—	0.00	○	○
$K\pi$	15.3 ± 3.3	23.3	3.51	○	○
$K\rho$	< 16.2	—	0.18	○	○
$K^*(1680)$, $\Gamma_{\text{exp}}^{\text{total}} = 322 \pm 110$ MeV					
$K^*(892)\pi$	96.3^{+33}_{-36}	44.5	1.27	○	○
$K\pi$	124.6 ± 42	107.7	2.71	○	○
$K\rho$	101.1^{+38}_{-35}	39.3	2.21	○	○
$K_2^*(1430)$, $\Gamma_{\text{exp}}^{\text{total}} = 105 \pm 10$ MeV					
$K^*(892)\pi$	24.3 ± 1.6	29.1	6.75	○	○
$K\pi$	49.1 ± 1.8	77.6	14.1	○	○
$K\rho$	8.5 ± 0.8	17.6	3.89	○	○
$K\omega$	2.9 ± 0.8	2.7	1.30	○	○
$K\eta$	$0.15^{+0.33}_{-0.10}$	3.4	0.06	○	○
$K_2^*(1980)$, $\Gamma_{\text{exp}}^{\text{total}} = 373 \pm 70$ MeV					
$K^*(892)\pi$	seen	—	0.00	○	○
$K\pi$	—	—	1.15	○	○
$K\rho$	seen	—	0.53	○	○

Table 11: Results on strong two-body decays of (excited) isodublet K_J^* mesons with $J = 0, 1, 2$. All widths are given in units of [MeV]; the experimental data are extracted from ref. [14]. For further comments, see text and caption of tab. 3.

Final State	Experimental Partial Width	3P_0 Model (Ref. [8])	This Work	incl. III	incl. ZRV
$K_3^*(1780)$, $\Gamma_{\text{exp}}^{\text{total}} = 159 \pm 21$ MeV					
$K\rho$	49.3 ± 15.7	30.0	9.17	○	○
$K^*(892)\pi$	31.8 ± 9.0	37.1	2.84	○	○
$K\pi$	29.9 ± 4.3	46.9	3.83	○	○
$K\eta$	47.7 ± 21.6	8.4	12.8	○	○
$K_2^*(1430)\pi$	< 25.4	—	0.14	○	○
$K^*(892)\rho$	—	—	44.3	○	○
$K^*(892)\omega$	—	—	14.8	○	○
$K_4^*(2045)$, $\Gamma_{\text{exp}}^{\text{total}} = 198 \pm 30$ MeV					
$K\pi$	19.6 ± 3.8	21.7	1.10	○	○
$K^*(892)\phi$	2.8 ± 1.4	—	1.13	○	○
$K_5^*(2380)$, $\Gamma_{\text{exp}}^{\text{total}} = 178 \pm 49$ MeV					
$K\pi$	10.9 ± 3.7	—	0.33	○	○

Table 12: Results on strong two-body decays of (excited) isodublet K_J^* mesons with $J = 3, 4, 5$. All widths are given in units of [MeV]; the experimental data are extracted from ref. [14]. For further comments, see text and caption of tab. 3.

Final State	Experimental Partial Width	3P_0 Model (Ref. [7])	This Work	incl. III	incl. ZRV
$\eta'(958)$, $\Gamma_{\text{exp}}^{\text{total}} = 0.20 \pm 0.02$ MeV					
$\rho\pi$	< 0.008	—	0.00	○	○
$\eta(1440)$, $\Gamma_{\text{exp}}^{\text{total}} = 50 \dots 80$ MeV					
KK^*	21.6 ± 5.2	—	21.8	○	○
$a_0(980)\pi$	26.6 ± 7.0	—	18.8	●	●
$\sigma\eta$	27.0 ± 6.0	—	43.9	●	●
$\eta_2(1645)$, $\Gamma_{\text{exp}}^{\text{total}} = 180^{+22}_{-20}$ MeV					
$a_0(980)\pi$	seen	—	20.8	○	○
$a_2(1320)\pi$	seen	189	18.5	○	○
KK^*	seen	26	5.18	○	○
$\rho\rho$	—	33	0.16	○	○

Table 13: Results on strong two-body decays of (excited) isoscalar η_J mesons. All widths are given in units of [MeV]. The experimental data for the $\eta(1440)$ partial widths are extracted from ref. [16]; the rest is given in ref. [14]. For further comments, see text and caption of tab. 3.

C.2 Figures

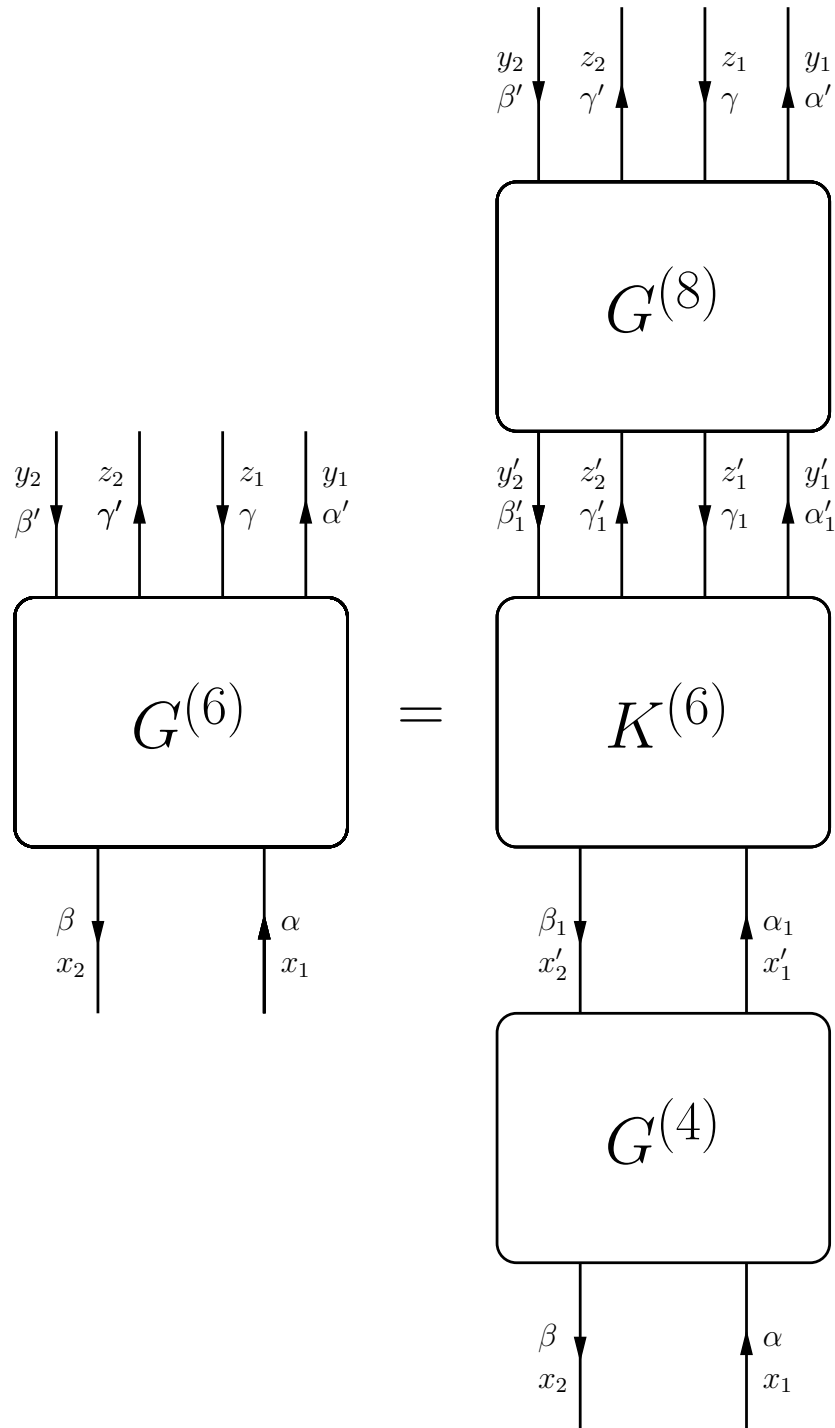


Figure 1: Decomposition of the six-point Green's function $G^{(6)}$ into the corresponding kernel $K^{(6)}$.

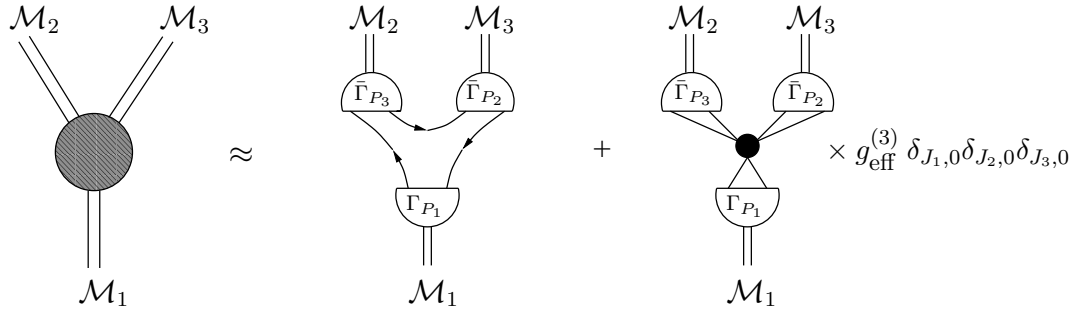


Figure 2: Diagrammatic illustration of the decay of one meson with four momentum P_1 into two other mesons with four momenta P_2 and P_3 via the full transition matrix element including quark loops and the instanton-induced six-quark vertex; note that the latter only contributes if all mesons in the decay have zero angular momentum. The quark loop diagram with the two outgoing mesons exchanged as well as the cyclic permuted diagrams of the instanton-induced transitions are suppressed in this figure.

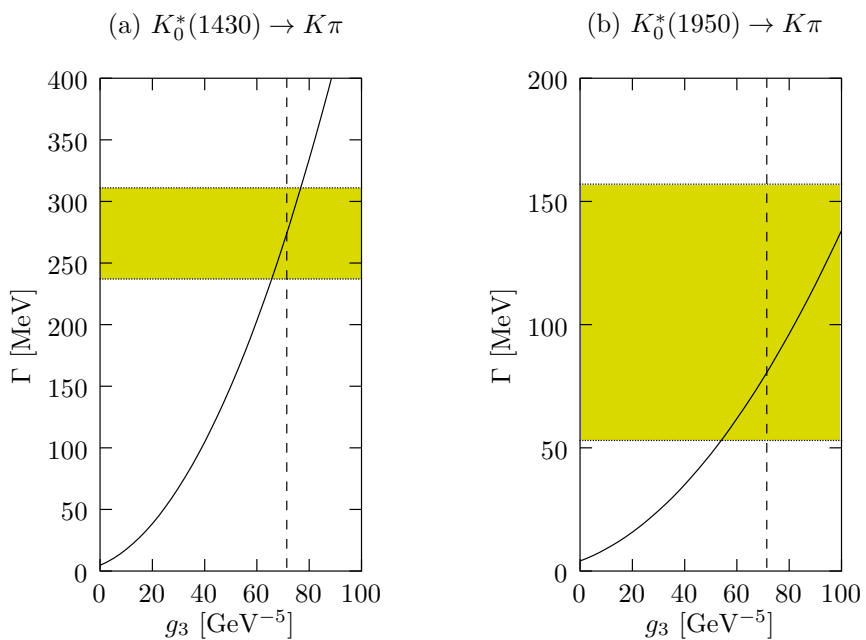


Figure 3: The widths of the decays (a) $K_0^*(1430) \rightarrow K\pi$ and (b) $K_0^*(1950) \rightarrow K\pi$ and their dependence on the coupling constant $g_{\text{eff}}^{(3)}$ of 't Hooft's three-body force due to instanton effects; see text for more details. The shaded bands denote the experimental error bars according to the PDG (see [14]); the vertical dashed lines mark our choice for the 't Hooft coupling $g_{\text{eff}}^{(3)}$.

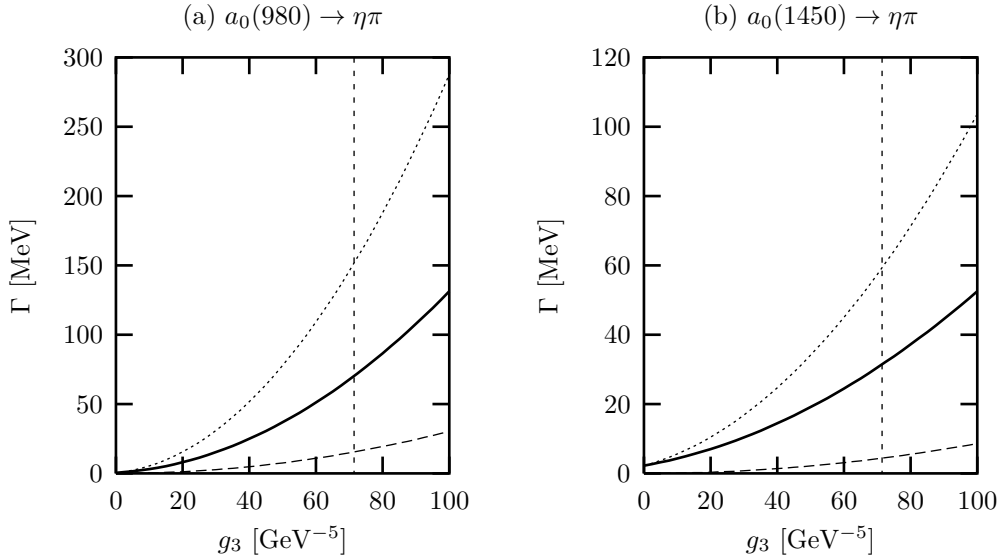


Figure 4: The widths of the decays (a) $a_0^*(980) \rightarrow \eta\pi$ and (b) $a_0^*(1450) \rightarrow \eta\pi$ and their dependence on the coupling constant $g_{\text{eff}}^{(3)}$ of 't Hooft's three-body force due to instanton effects; see text for more details. The fat solid line (—) indicates the total decays widths based on the interference of OZI allowed diagrams (---) and OZI violating diagrams due to the instanton interaction (···); obviously, the interference in this example is destructive. Again, the vertical dashed lines mark our choice for the 't Hooft coupling $g_{\text{eff}}^{(3)}$.

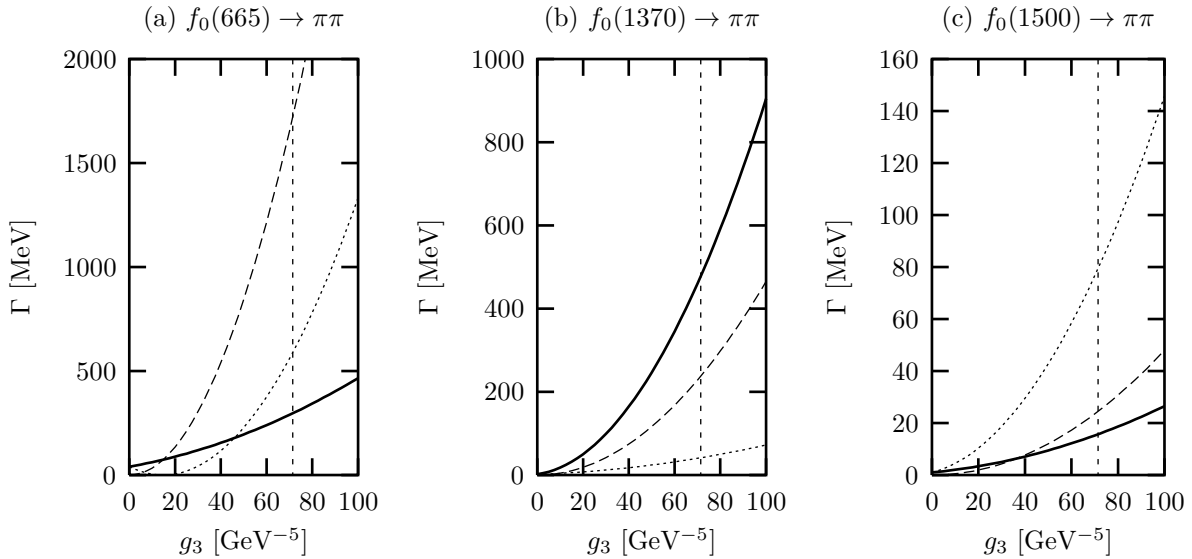


Figure 5: The widths of the decays $f_0 \rightarrow \pi\pi$ and their dependence on the coupling constant $g_{\text{eff}}^{(3)}$ of 't Hooft's three-body force for (a) the ground state with $M_{f_0} \approx 400 \dots 1200$ MeV ≈ 665 MeV, (b) the first radial excitation with $M_{f_0} \approx 1370$ MeV, and (c) the second radial excitation with $M_{f_0} \approx 1500$ MeV; see text for more details. Again, the fat solid line (—) indicates the total decays widths based on the interference of OZI allowed diagrams (---) and OZI violating diagrams due to the instanton interaction (···). Here as in the other pictures, the vertical dashed lines mark our choice for the 't Hooft coupling $g_{\text{eff}}^{(3)}$.

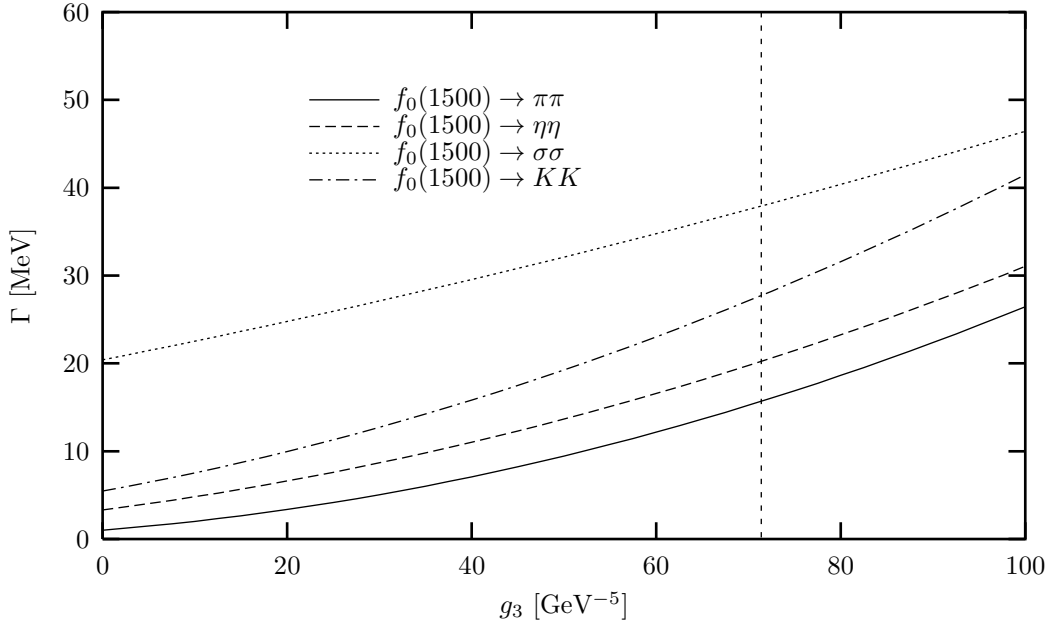


Figure 6: The widths of the decays $f_0(1500) \rightarrow \pi\pi$, $f_0(1500) \rightarrow \eta\eta$, $f_0(1500) \rightarrow \sigma\sigma$ and $f_0(1500) \rightarrow KK$, and their dependence on the coupling constant $g_{\text{eff}}^{(3)}$ of 't Hooft's three-body force; see text for more details. The vertical dashed lines mark our choice for the 't Hooft coupling $g_{\text{eff}}^{(3)}$.

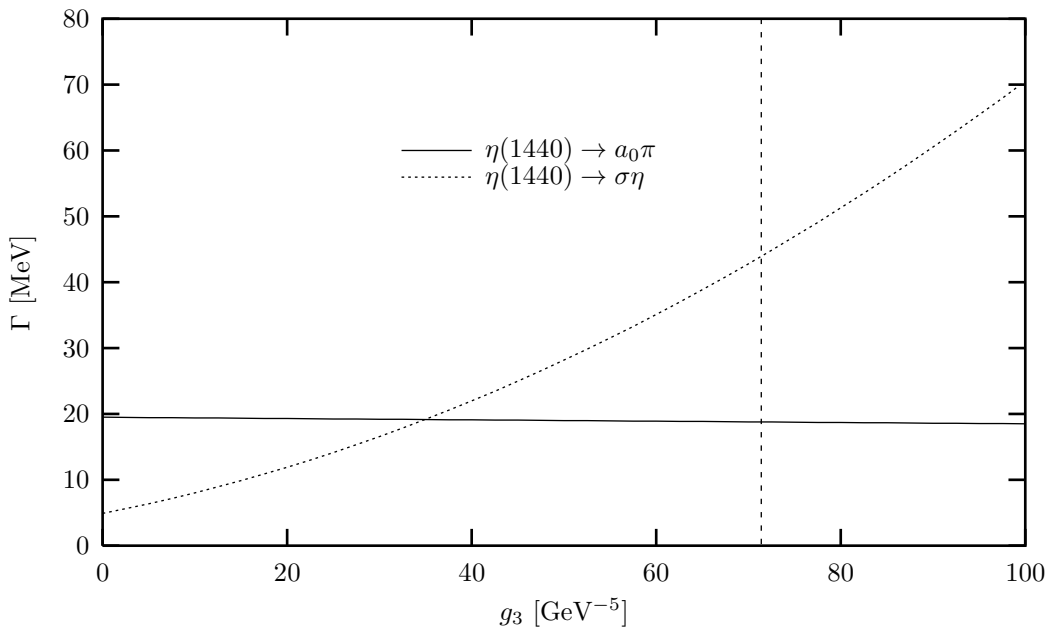


Figure 7: The widths of the decays $\eta(1440) \rightarrow a_0^*(980)\pi$ and $\eta(1440) \rightarrow \sigma\eta$ and their dependence on the coupling constant $g_{\text{eff}}^{(3)}$ of 't Hooft's three-body force due to instanton effects; see text for more details. Note that the vertical dashed line denotes our choice for the 't Hooft coupling $g_{\text{eff}}^{(3)}$.